Reentrant Glass Transition In Suspensions of Colloidal Ellipsoids

A Thesis submitted in partial fulfillment

for the degree of

MASTER OF SCIENCE

as a part of the

Integrated Ph.D. programme

(Materials Science)

by

Chandan Kumar

CHEMISTRY AND PHYSICS OF MATERIALS UNIT
JAWAHARLAL NEHRU CENTRE FOR ADVANCED SCIENTIFIC RESEARCH
Bangalore – 560 064, India

APRIL 2013

To My Grandparents

DECLARATION

I hereby declare that the matter embodied in the thesis entitled "**Reentrant Glass Transition In Suspensions of Colloidal Ellipsoids**" is the result of investigations carried out by me at the Chemistry and Physics of Materials Unit, Jawaharlal Nehru Centre for Advanced Scientific Research, Bangalore, India under the supervision of Dr. Rajesh Ganapathy and that it has not been submitted elsewhere for the award of any degree or diploma.

In keeping with the general practice in reporting scientific observations, due acknowledgement has been made whenever the work described is based on the findings of other investigators. Any omission that might have occurred by oversight or error of judgement is regretted.

Chandan Kumar

CERTIFICATE

I hereby certify that the matter embodied in this thesis entitled "**Reentrant Glass Transition In Suspensions of Colloidal Ellipsoids**" has been carried out by Mr. Chandan Kumar at the Chemistry and Physics of Materials Unit, Jawaharlal Nehru Centre for Advanced Scientific Research, Bangalore, India under my supervision and that it has not been submitted elsewhere for the award of any degree or diploma.

Dr. Rajesh Ganapathy
(Research Supervisor)

Acknowledgements

When I look back to my school days, I find that I was mentally trained to be a defence personnel with science just as an alternative career option but two years of my stay in Soft Matter Lab has changed the way I perceive science and especially research. I express my deepest gratitude to my supervisor, Dr. Rajesh Ganapathy for bringing this change in me. I am thankful to him for suggesting a very exciting and challenging problem for my MS project. He has not only given me the freedom to explore things but also provided constant support and encouragement throughout the project.

I sincerely thank the earlier and present Chairman of CPMU, Prof. G.U. Kulkarni and Prof. S. Balasubramanian for giving me an opportunity to pursue science in JNCASR. I also thank the earlier and present Coordinators of Int. PhD programme, Prof. S. Balasubramanian and Dr. T.K. Majhi for their guidance and support. I always cherish the fatherly love and care which I received from "Bala Sir".

I thank Prof. C. N. R. Rao, FRS, for providing excellent research facilities and being as a constant source of inspiration.

I convey my special thanks to my collaborator Amritha Rangarajan, for taking the initiation in the synthesis of ellipsoidal particles in the lab, without which this project would have not been possible.

With warm regards, I thank Prof. Chandan Das Gupta, Prof. Alok Nath Chakravarty, Dr. Jaydeep Basu, Prof. S. Balasubramanian, Prof. Chandrabhas,

Prof. K.S. Narayana, Prof. G.U. Kulkarni, Prof. A. Sundaresan, Prof. S.M. Shivaprasad, Dr. Sridhar Rajaram, Dr. Rajesh Ganapathy, Dr. M. Ishwarmoorthy, Dr. Ranjan Dutta, Dr. Subir K. Das, Prof. S. K. Pati, Prof. Umesh Waghmare, Prof. Shobhana Narasimhan, Prof. H. Ila, Dr. A. Govindraj. I express my gratitude to all these professors who have taught me various courses over the last three years of my stay in JNC.

I thank all the teaching assistants - Narendra, Malli Tangi, Varun, Pralok, Nisha, Kanchan, Nitesh, Raju, Sandeep for helping with my course work.

I also thank all my lab mates Manasa, Srishti, Amritha, Rajeev, Neelima, Vikram and Shreyas for being supportive and helping me as and when needed. My special thanks to Manasa for making me adapt to lab and research environment and Srishti for making my stay in the lab enlivening and cheerful.

My heart felt thanks to all my friends - Deepak, Chandan De, Rajsekhar, Anirban, Sisir, Koushik, Ankush, Rajesh Singh, Ram, Adhip, Anurag, Harsh Bana, Abhishek, Maria, Dhanya, Dibo Da, Arjun, Ramana, Sunil, Rajdeep, Wasim, Pallavi, Raagesh, Renu, Arkamita. They have stayed with me in my happy and sad times.

I thank all my teachers from college and school - Mr. S.V. Bakre, Dr. V. P. Nagpal, Dr.Pragati Ashdhir, Dr. J.S. Bisht, Mr. G.S. Joshi, Mr. K.N. Joshi, Mr. A.C. Rai, Mr. A.K. Srivastava, Mrs. Meena Srivastava for their encouraging words and motivation during my formative years.

I appreciate all the efforts of JNC staffs - academic, administrative, library, technical and hostel for making my stay comfortable.

Last but not the least, I am deeply grateful to my family for their immense support and a firm belief in all my decision pertaining to career.

Preface

This thesis is divided into three chapters.

The first chapter gives a brief overview to glass transition and glasses and the role of colloids in understanding these phenomena. We have also discussed our motivation for studying the reentrant glass dynamics of short colloidal ellipsoids.

The second chapter contains a detailed discussion on material and methods.

In the last chapter, we have discussed the glass transition dynamics in quasi-2 dimensional suspensions of colloidal ellipsoids, aspect ratio $\alpha = 2.1$, with repulsive as well as attractive interactions. For the purely repulsive case, we found that the orientational and translational glass transitions occur at the same area fraction. The reentrant glass dynamics which is well understood for spherical particles with symmetric interaction, has been explored for the colloidal ellipsoids with anisotropic short-range attraction. Strikingly, for intermediate attraction strengths, we found that the orientational glass transition precedes the translational one. We have quantified the structure and dynamics to rationalize our observations. We show that quasi-long range ordering is promoted at intermediate attraction strengths which subsequently results in a two-step glass transition. Most interestingly, within experimental certainty, we observe reentrant glass dynamics only in the translational degrees of freedom.

Contents

Acknowledgements **v**

Preface **vii**

1 Introduction **1**

1.1 Glass Transition and Glasses 1

1.2 Mode Coupling Theory (MCT) and Glass Transition 3

1.2.1 Prediction 1 4

1.2.2 Prediction 2 5

1.2.3 Prediction 3 6

1.3 Hard Particle Models 6

1.4 Colloids as Model Systems to Study Glass Transition 9

1.4.1 Colloidal Suspensions 9

1.4.2 Colloidal Glass Transition and Glasses 10

1.5 Attractive Glasses 16

1.6 Shape Anisotropy and the Glass Transition 20

1.7 Motivation for the Present Work 25

Bibliography **27**

2 Experimental **33**

2.1 Synthesis of PS Spheres 33

2.2 Synthesis of PVA 34
2.3 Film Formation and Ellipsoid Synthesis 35
2.4 Experimental Cell and Imaging 38

Bibliography **41**

3 Depletion Attraction Induced Two-Step Glass Transition in Short Colloidal Ellipsoids **43**

3.1 Ellipsoids with Purely Repulsive Interactions 44
3.2 Hard Ellipsoids with Depletion Induced Attractive Interactions 54
3.3 Reentrant Glass Dynamics in Hard Ellipsoids 59
3.4 Rationalising Our Observations 63

Bibliography **69**

List of Publications **73**

List of Figures

1.1 Different ways a liquid (red curve) can be transformed to a solid is shown in (V, T) plane at a constant pressure. If the liquid is cooled slowly, it crystallizes below the freezing point (the green curve). If the same liquid is cooled rapidly (blue curve), it bypasses crystallization and passes through a glass transition regime and falls out of equilibrium below T_g. The dependence of T_g on rate of cooling is also shown. Adopted from.[4] 2

1.2 Self intermediate scattering function $F_s(q, t)$ at various temperatures T. The β and α-relaxation regimes are shown. Adopted from.[14] . . . 4

1.3 The collapse of $F_s(q, t)$ on a master curve (dashed line) in the α-relaxation regime obtained from von Schweilder law for a Lennard-Jones binary system. The time axis has been rescaled with τ_α. The temperature in K (from left to right): 5.0, 4.0, 3.0, 2.0, 1.0, 0.8, 0.6, 0.55, 0.5, 0.475 and 0.466. Adopted from.[17] 6

1.4 Hard sphere interaction potential (red color) as a function of r. . . . 7

1.5 Hard sphere phase diagram as a function of volume fraction Φ. Adopted from.[19] 8

1.6 (a) Colloidal suspension (b) Spherical colloidal particles in a refractive index matched solvent. Hence they are not visible in isotropic phase but they show Bragg scattering in the crystalline phase at the bottom. Adopted from.[33] 9

1.7 Nearly hard spheres colloidal suspension, 4 days after tumbling. States of the suspensions from left, first - fluid; next three - liquid-crystal coexistence; next two - homogeneous crystal; 7^{th} - heterogeneous crystal; last two - glass. Bragg scattering can be observed in crystalline samples. The last sample did not crystallize even after several months. Adopted from.[47] 11

1.8 Semilogarithmic plot of $F_s(q,t)$ with delay time τ for different samples. A - fluid; C* - fluid-fluid coexistence; B, C, D - fluid-crystal coexistence; E, F - crystals; G, H, I, J - glass. Adopted from.[48] 12

1.9 (A) $\langle \Delta r^2 \rangle$ at various volume fraction Φ as indicated in the plot. The solid line has slope 1. (B) The non-Gaussian parameter $\alpha_2(t)$ and (C) the particle avergared cluster size of fast particles, $\langle N_c \rangle$ with time. The Φs in (B) and (C) are color coded as in (A). The dashed line shows the expected result for random distribution of fast particles. Adopted from.[50] 13

1.10 The probability distribution of displacements, $(P(\Delta r(t)))$, over t^* for $\Phi = 0.56$. The dashed line is best fit Gaussian, the solid line is a stretched exponential fit to the tails of the distribution. The particles within dotted lines are slowest 95%. Adopted from.[50] 15

1.11 Spatial distribution of clusters fastest particles (large spheres). For clarity, the slowest (95% of the particles are shown as small spheres in the background. (A) Supercooled liquid at $\Phi = 0.56$. (B) Glass at $\Phi = 0.61$. Particles belonging to the same clusters are shown in same color. Adopted from.[50] 15

1.12 The variation of $\langle N_c \rangle$ with Φ. The dashed horizontal line indicates $\langle N_c \rangle$ for random distribution of fast particles. The vertical dashed line represents Φ_g. Adopted from.[50] 16

1.13 Phase diagram for a square-well system with square well of relative width $\varepsilon = 0.03$. The inset shows the phase diagram, where AGL and RGL are shown at various ε. Adopted from.[66] 17

1.14 Depletion attraction. Left - Schematic of colloid-polymer suspension. Excluded volume (light gray) around each colloidal particle, polymer molecules with radius of gyration, r_g and red region represent the overlap of excluded volume leading to attraction between particles. Right - Schematic of depletion induced attractive potential. Adopted from.[69] 19

1.15 $F_s(q,t)$ as a function of time, t, at various depletion concentration at a fixed Φ. sample A - repulsive glass, sample B - ergodic fluid, sample C, D and E - attractive glass. Adopted from.[31] 19

1.16 Phase diagram of colloid-polymer mixture in (c_p, Φ) plane. Open symbols represent thermally equilibrated samples: fluids (triangles), fluid-crystal coexistence (diamonds), fully crystalline (inverted triangles). Solid symbols represents non-equilibrated samples: repulsion driven glass (circles), attraction driven glass (squares). dashed curves are guide to the eye for observed glass transition. Solid lines are MCT predicted glass transition lines. Adopted from.[31] 20

1.17 Phase diagram of uniaxial hard ellipsoids in (Φ, α) plane. Solid symbols corresponds to fluid-solid transition, hollow symbol corresponds to isotropic-nematic transition. The black (dark) line is maximum achievable density.[83] Cyan (light gray) dashed lines and blue (dark) dashed lines are guides to the eye which join the fluid-solid and isotropic-nematic transitions, respectively. The cyan (light gray) solid lines indicate fcc-SM2 transitions.[79] Black (dark) plus symbols (isotropic-nematic) and asterisks (nematic-solid) are taken from the.[78] The inserted snapshots are placed according to the phase diagram region. Particles are colored according to their orientations by setting red, blue, and green to given orthogonal directions, and using a linear combination for intermediate cases. Adopted from.[82] 22

1.18 ${\tau_\alpha}^{-1/\gamma}$ *vs* ϕ. Open and solid symbols correspond to orientational and translational DOF, respectively. Dashed and solid lines are linear fits to the data. Adopted from.[85] 23

1.19 The spatial distribution of rotational (b, d, f) and translational (a, c, e) most-mobile particles of the system. (a), (b) at $\phi = 0.70$ (supercooled liquid); (c), (d) at $\phi = 0.77$ (orientational glass); (e), (f) at $\phi = 0.81$ (glass). ellipsoids in same cluster have same color. Adopted from.[85] 24

1.20 Two radii of curvature for the ellipsoids; R_{big} and R_{small}. When depletion attraction is turned on, due to anisotropy configuration 1 is preferred over 2. 25

2.1 Unstretched PVA film with PS spherical particles embedded in it. The red lines marks the square grids of size 0.5 cm x 0.5 cm. 35

2.2 Stretching apparatus built in our lab. The film is clamped in between two steel blocks as shown and stretching is done manually. 36

2.3 Stretched film. The square grids prior to stretching have changed to rectangles depending on the draw ratio. 36
2.4 FESEM images of the ellipsoids. The scale bar is 5 μm. 37
2.5 Schematic of the wedge cell with ellipsoids (blue color) loaded in it. The thin regions of the cell are quasi 2-dimensional (not to scale). . . 38
2.6 (a) Out-of-plane orientations of ellipsoid in a thick cell and their projections in the imaging plane. Distribution of the change in major axis Δl (b) minor axis Δw (c) of the ellipsoids between successive frames. The solid lines represents Gaussian fits to the distribution. . . 39
2.7 The image shows the tracking of the ellipsoid at $\phi = 0.79$. The red lines are the boundaries of the ellipsoids which have been drawn with the information obtained from Image-J 39
2.8 (a) $\langle \Delta r^2 \rangle$ *vs.* t at $\phi = 0.04$ and (b) $\langle \Delta \theta^2 \rangle$ *vs.* t at $\phi = 0.04$ for estimating the spatial and orientational resolution. 40

3.1 Representative image of colloidal ellipsoids at $\phi = 0.79$. 44
3.2 Self intermediate scattering function $F_s(q = 5.6\mu m^{-1}, t)$ at various area fractions ϕ. 45
3.3 Dynamic orientational correlation function $L_5(t)$ at various area fractions ϕ. 46
3.4 ${\tau_\alpha}^{-1/\gamma}$ *vs* ϕ. Here, $\gamma^T = 1.93$ and $\gamma^R = 2.04$. Dashed and solid lines are power law fits to the data, respectively. 47
3.5 $\langle \Delta r^2 \rangle$ at various ϕ. The solid line has slope 1 and the dashed horizontal line represents the minimum tracking resolution in our experiments. 48
3.6 $\langle \Delta \theta^2 \rangle$ at various ϕ. The solid line represent the line of slope 1. 49
3.7 Non-Gaussian parameter $\alpha_2^T(t)$ (a) and $\alpha_2^R(t)$ (b) at various ϕ. 50
3.8 $P(\Delta r)$ *vs* Δr over t^* at three ϕ's in the vicinity of ϕ_g. Here t^* corresponds to the cage breaking time. 50

3.9 Top 10 % translationally most-mobile (open blue circles) and orientationally most-mobile (solid red circles) particles at $\phi = 0.79$. 51

3.10 Average cluster size, $\langle N_c \rangle$ at different ϕ's. The vertical dashed line represents the glass transition area fraction ϕ_g 52

3.11 Divergence of average cluster size: $\langle N_c \rangle$ *vs* $(\phi_g - \phi)$. 53

3.12 The scaling of relaxation time, τ_α with $(1 - (\phi/\phi_0))$. The inset shows the residuals of the linear fits as a function of the fitting parameter ϕ_0. The dashed vertical line corresponds to ϕ_g for purely repulsive ellipsoids. The solid vertical line represents the average value of ϕ_0. . 54

3.13 Image shows lateral alignment being promoted with turning on short-range depletion attraction 55

3.14 Distribution of dimer lifetimes for (a) $c_p = 10$ μgml^{-1} (b) $c_p = 40$ μgml^{-1} (c) $c_p = 50$ μgml^{-1}. The solid line in (b) and (c) shows exponential fits to the data. (d) Log-Linear plot of $\tau_0 D$ *vs* c_p. The solid line is linear fit to the data from which $\tau_0 D$ at $c_p = 30$ μgml^{-1} was obtained. 56

3.15 $\langle \Delta r^2 \rangle$ at different ϕ's and for $\Delta u = 0.44$ (a) $\Delta u = 1.16$ (b) $\Delta u = 1.47$ (c) $\Delta u = 1.95$ (d) The $\langle \Delta r^2 \rangle$ at $\phi = 0.67$ and $\phi = 0.72$ in (c) were observed to be same. The faster dynamics at $\phi = 0.72$ is attributed to thicker cell area in the viewing region.The solid lines in all sub-plots represent line of slope 1. 57

3.16 $\langle \Delta \theta^2 \rangle$ at different ϕ's and for $\Delta u = 0.44$ (a) $\Delta u = 1.16$ (b) $\Delta u = 1.47$ (c) $\Delta u = 1.95$ (d) The $\langle \Delta \theta^2 \rangle$ at $\phi = 0.67$ and $\phi = 0.72$ in (c) were observed to be same. The faster dynamics at $\phi = 0.72$ is attributed to thicker cell area in the viewing region. The solid lines in all sub-plots represent line of slope 1. 58

3.17 $F_s(q = 5.6\mu m^{-1}, t)$ and (b) $L_3(t)$ for $\Delta u = 0$ at $\phi = 0.79$ (black squares), $\Delta u = 1.16$ at $\phi = 0.81$ (red circles), $\Delta u = 1.47$ at $\phi = 0.81$ (green triangles). Inset to (a) and (b) - with expanded y-axis show two-step relaxation. Solid and open symbols correspond to orientational and translational scaling of τ_α, respectively. 59

3.18 MCT scaling of τ_α for $\Delta u = 0.44$ (a), $\Delta u = 1.16$ (b), $\Delta u = 1.47$ (c) and $\Delta u = 1.95$ (d). Solid and open symbols correspond to orientational and translational scaling of τ_α, respectively. The lines are linear fits to the data. The solid and dashed vertical lines in (c) and (d) denote ${\phi_g}^R$ and ${\phi_g}^T$ respectively. 60

3.19 Phase diagram in $(\Delta u, \phi)$ plane. The circles represent the Δu and ϕ at which experiments were performed. (a) Translational DoF. (b) Orientational DoF. The black circles denote $F_s(q, t_\infty)$ and $L_3(t_\infty)$ that decayed completely. The white circles denote $F_s(q, t_\infty)$ and $L_3(t_\infty)$ that decayed partially. The color bar indicates the value of $\alpha_2(t = t^*)$. $\alpha_2^{T,R}(t^*)$ for ϕ's in between experimental data points were obtained from linear interpolation. Note the break in ϕ-axis at $\phi \approx 0.53$. ${\phi_g}^T$ and ${\phi_g}^R$, obtained from MCT scaling analysis, are shown by squares in (a) and (b) respectively. 62

3.20 Representative image of the gel phase at $\phi = 0.47$ and $\Delta u = 1.95$. . . 63

3.21 Representative images showing structure at (a) $\Delta u = 0$ at $\phi = 0.79$, (b) $\Delta u = 1.16$ at $\phi = 0.81$ and (c) $\Delta u = 1.47$ at $\phi = 0.81$. 64

3.22 Pair correlation function $g(r)$ for $\Delta u = 0$ at $\phi = 0.79$ by black squares, $\Delta u = 1.16$ at $\phi = 0.81$ by red circles, and $\Delta u = 1.47$ at $\phi = 0.81$ by cyan triangles. 65

3.23 Static orientational correlation function $g_2(r)$ for $\Delta u = 0$ at $\phi = 0.79$ by black squares, $\Delta u = 1.16$ at $\phi = 0.81$ by red circles, and $\Delta u = 1.47$ at $\phi = 0.81$ by cyan triangles. 66

3.24 Ratio of mean-squared displacements along major and minor axis of ellipsoids for $\Delta u = 0$ at $\phi = 0.79$ by black squares, $\Delta u = 1.16$ at $\phi = 0.81$ by red circles, and $\Delta u = 1.47$ at $\phi = 0.81$ by cyan triangles. 67

3.25 Top 10 % orientationally (solid) and translationally (hollow) most-mobile particles at $\Delta u = 1.16$ and $\phi = 0.81$. 68

Chapter 1

Introduction

1.1 Glass Transition and Glasses

The microscopic underpinnings of glasses and the glass transition continue to remain one of the grand challenges in condensed matter physics.[1–3] It is well known that when a liquid is cooled slowly, at its freezing temperature, T_f, it transforms to a crystalline state (Figure 1.1). However, if the same liquid is cooled rapidly, crystallization can be bypassed at T_f and the liquid can be supercooled and with further supercooling, at glass transition temperature, T_g, the liquid falls out of equilibrium (Figure 1.1). Associated with this transition, there is onset of an elastic modulus with almost no discernible change in structure. The system below T_g is called glass. These experimental observations raise a few interesting questions,

1. *Is this a phase transition?*

2. *What leads to slowing down of relaxation with almost no change in structure?*

3. *It is well known that particle dynamics in supercooled liquids and glasses are heterogeneous. What is the origin of dynamical heterogeneity?*

4. *Does particle shape and interaction potential have any role in the physics of the glass transition?*

In-spite of continued efforts to address these questions, there is no consensus on

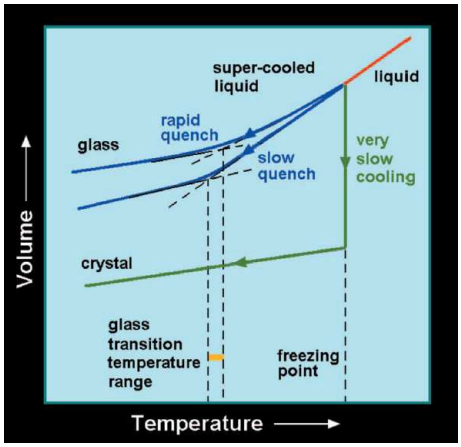

Figure 1.1: Different ways a liquid (red curve) can be transformed to a solid is shown in (V, T) plane at a constant pressure. If the liquid is cooled slowly, it crystallizes below the freezing point (the green curve). If the same liquid is cooled rapidly (blue curve), it bypasses crystallization and passes through a glass transition regime and falls out of equilibrium below T_g. The dependence of T_g on rate of cooling is also shown. Adopted from.[4]

the physics of the glass transition. Interestingly, T_g depends on the rate of cooling itself (Figure 1.1).[2,4] Conventionally, T_g is defined as the temperature at which the viscosity, η, of the system reaches to the order of 10^{13} Poise.

There are many competing theories to explain this phase transition. The free volume theory[5,6] by Cohen and Turnbull (1959) attributes the glass transition to the drastic decrease in free volume v_f which ceases the diffusive motion of particles. The thermodynamic theory[7,8] by Adams and Gibbs (1965) predicts the glass transition as a second order phase transition and associates it with decrease in configurational entropy of the system. There are kinetic theories[9,10] which do not consider T_g to be a thermodynamic variable and are mainly concerned with rate of approach to the glass transition. Another theory which is more appealing to an experimentalist is the mode coupling theory (MCT) whose predictions can be tested in experiments. Here, we will briefly discuss the predictions of MCT.

1.2 Mode Coupling Theory (MCT) and Glass Transition

MCT was proposed by Bengtzelius, Gotze and Sjolander[11] and independently by Leutheeusser[12] in 1984. It aims to understand the slowing down of the dynamics from the liquid side and describes the glass transition as a dynamical crossover to a structurally arrested state at the temperature T_c. Using, the mode coupling approximations, equations of motion of a dense liquid were described in terms of density fluctuations of the system. The solutions to these equations predicted the cage-effect, a given particle is trapped in the cage formed by its nearest neighbours and it takes a finite time for the particle to escape, as the primary mechanism for the motion of particle in supercooled liquids. As T_c is approached, the strength of caging increases and the structural relaxation time τ_α diverges. The MCT predicted T_c is typically greater than T_g due to unaccounted hopping processes near the glass transition in the MCT formalism.[13]

The dynamic evolution of density fluctuations $\rho(q,t)$ for a given wave vector q in a liquid is described by the self intermediate structure factor $F_s(q,t)$ which can be measured in scattering experiments or computer simulations.

$$F_s(\mathbf{q},t) = \frac{\langle \delta\rho^*(\mathbf{q},t)\delta\rho(\mathbf{q},t)\rangle}{N}$$
$$\rho(q,t) = \sum_{j=1}^{N} \exp[i\mathbf{q}\cdot\mathbf{r}_j(t)]$$

Here, N is the total number of particles, $\mathbf{r}_j(t)$ is the position of j^{th} particle at time t and $\langle\rangle$ denotes the time averaging. The static measurement of $F_s(q,t)$ gives the structure factor $S(q)$ which is the Fourier transform of particles' position in real space,

$$S(q) = F_s(q,0) = \frac{\langle \sum_{jk} \exp[i\mathbf{q}\cdot(\mathbf{r}_j - \mathbf{r}_k)]\rangle}{N}$$

where the sum is done over the pair of particles j and k of the system, r_j and r_k are coordinates of j^{th} and k^{th} particles. A typical relaxation curve for $F_s(q,t)$ is

shown in Figure 1.2 below. The decay is exponential at high temperature where

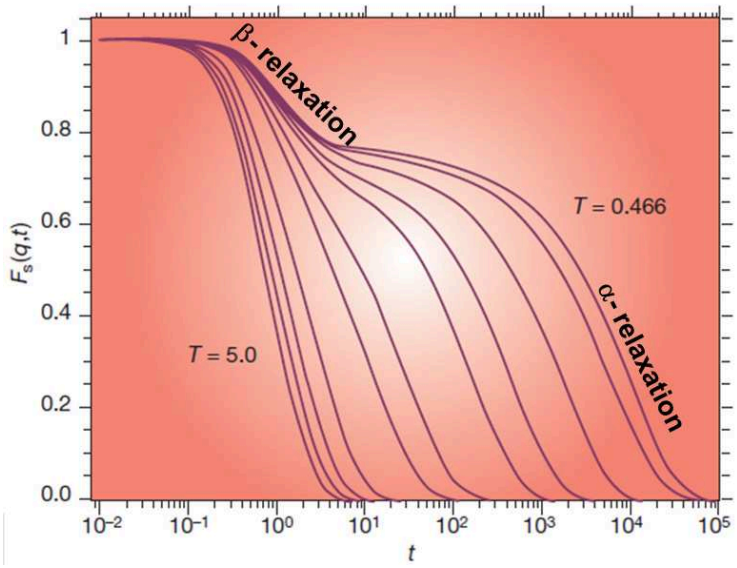

Figure 1.2: Self intermediate scattering function $F_s(q,t)$ at various temperatures T. The β and α-relaxation regimes are shown. Adopted from.[14]

the motion of particles is diffusive. At low T, $T > T_c$, i.e. for supercooled liquids, a two-step relaxation is observed. While the first step corresponds to rattling of particles inside the cages formed by neighbouring particles (the β-relaxation), the second one corresponds to the cage rearrangements and escape of the particles from their respective cages (the α-relaxation).[15,16] MCT predicts the behaviours of these relaxations and estimates T_c, from relaxation times. The three major predictions of MCT,[11,15–18] for $T \to T_c$ from liquid side, are given below.

1.2.1 Prediction 1

The relaxation in early β regime follows the critical power law behaviour,

$$F_s(q,t) = f_q + h_q(\tfrac{t}{t_\sigma})$$

where f_q is the plateau height, h_q is the amplitude and t_σ is given by,

$$t_\sigma = \tfrac{t_0}{|\sigma|^{1/2a}}$$

where t_0 is a system universal constant, a is the power law exponent and σ is the separation parameter given by,

$$\sigma = C(T - T_c)$$

where as discussed T_c is the mode coupling dynamical glass transition temperature. Hence, the intercept on T axis in the plot of ${t_\sigma}^{-2a}$ *vs.* T yields T_c.

1.2.2 Prediction 2

The relaxation in late β and early α regime follows the von Schweilder law i.e.

$$F_s(q,t) = f_q - h_q t^b$$

where f_q is the plateau height, h_q is the amplitude and b is a universal exponent called Schweilder exponent. The long time decay of $F_s(q,t)$ follows stretched exponential and yields structural relaxation time, τ_α,

$$F_s(q,t) = f exp[-(t/\tau_\alpha)^\beta]$$

Here β is an exponent. The structural relaxation time τ_α diverges as power law on approaching T_c,

$$\tau_\alpha(T) \propto (T - T_c)^{-\gamma}$$

where γ is a scaling exponent given by,

$$\gamma = \frac{1}{2a} + \frac{1}{2b}$$

Here a and b are power law and Schweilder exponent, respectively. Further, a and b are system universal parameter and are related as,

$$\frac{\Gamma(1-a)^2}{\Gamma(1-2a)} = \frac{\Gamma(1+b)^2}{\Gamma(1+2b)}$$

Hence, intercept on T axis in the plot of ${\tau_\alpha}^{-1/\gamma}$ vs. T yields T_c.

1.2.3 Prediction 3

$F_s(q,t)$ at different temperatures when scaled by their respective τ_α, collapse on a master curve in the α-relaxation regime (Figure 1.3). This is called as the time-temperature superposition principle (TTSP).

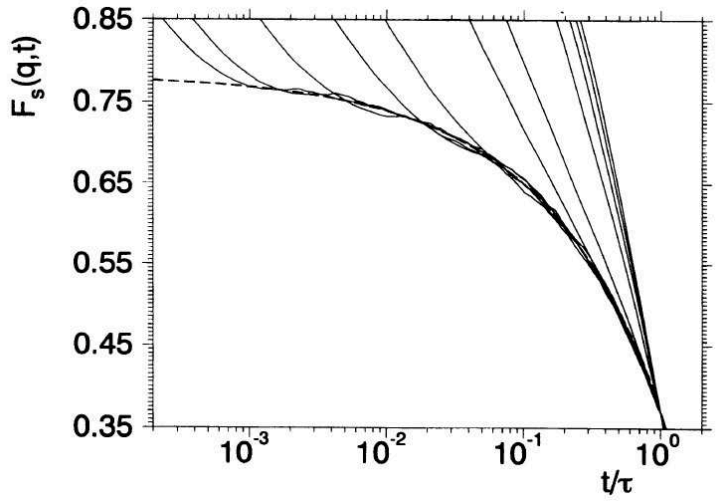

Figure 1.3: The collapse of $F_s(q,t)$ on a master curve (dashed line) in the α-relaxation regime obtained from von Schweilder law for a Lennard-Jones binary system. The time axis has been rescaled with τ_α. The temperature in K (from left to right): 5.0, 4.0, 3.0, 2.0, 1.0, 0.8, 0.6, 0.55, 0.5, 0.475 and 0.466. Adopted from.[17]

The parameters discussed in MCT predictions are easily accessible in scattering and optical experiments and hence, its validity can be tested. For hard spheres MCT predicts the glass transition at $\Phi = 0.52$, where Φ is the volume fraction.

1.3 Hard Particle Models

The interaction potential between colloidal particles is modelled as hard particle interaction i.e. for the spherical particles the potential U_{HS} is given as,

$$U_{HS} = \infty \text{ if } 0 < r < \sigma$$

$$U_{HS} = 0 \text{ if } r > \sigma$$

where σ is the diameter of the colloidal particle and r is the centre-to-centre distance between two particles. The hard sphere potential is schematically shown in Figure 1.4. From thermodynamics, the free energy F can be expressed in terms of

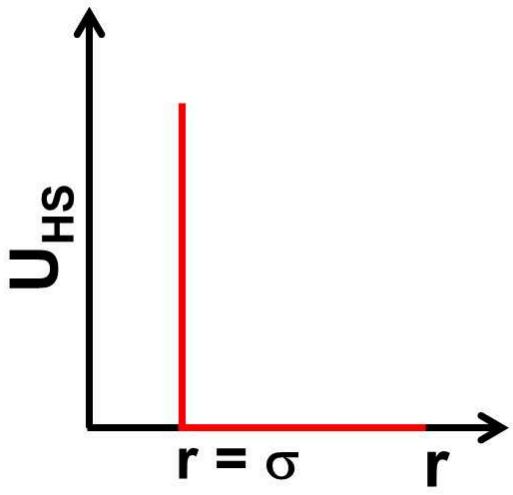

Figure 1.4: Hard sphere interaction potential (red color) as a function of r.

partition function, Z, summed over all configurations of the system.

$$F = U - TS = -k_B T \ln Z$$
$$Z = \sum_{config.} \exp(-\sum_{i,jbonds} \frac{U_{ij}}{k_B T})$$
$$\exp(-\sum_{i,jbonds} \frac{U_{ij}}{k_B T}) = 0 \text{ if } r \leq \sigma$$
$$\exp(-\sum_{i,jbonds} \frac{U_{ij}}{k_B T}) = 1 \text{ if } r \geq \sigma$$

where k_B is Boltzmann constant, T is temperature, U and S are the internal energy and the entropy of the system, respectively. Hence, *only* entropy governs the phase behaviour of hard sphere model. Entropy, for monodisperse hard spheres of radius a, depends on volume fraction, Φ. Thus, for hard spheres Φ acts like an inverse of temperature.

$$\Phi = \frac{4}{3}\pi a^3 \frac{N}{V}$$

where N is the total numbers of particles in a given volume V. The hard spheres phase diagram is shown in Figure 1.5.

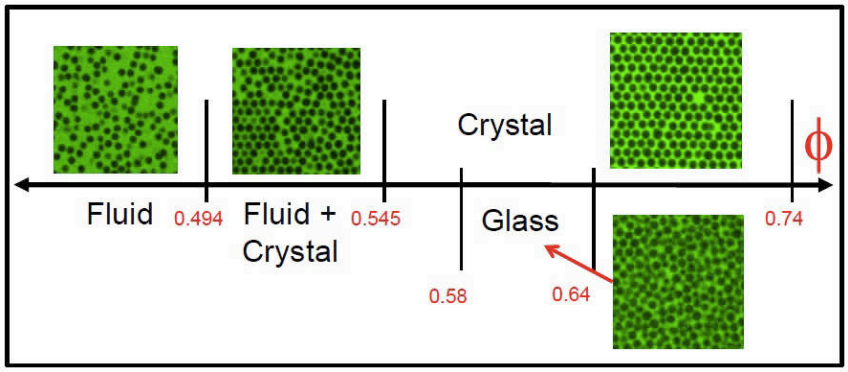

Figure 1.5: Hard sphere phase diagram as a function of volume fraction Φ. Adopted from.[19]

Before moving on to colloidal glasses and glass transition, it is important to note that colloidal systems differ from their atomic counterparts in many ways.[20,21] While the short time dynamics are ballistic in atomic systems, they are diffusive for colloidal systems. Further, the role of hydrodynamic couplings in dense colloidal suspensions are not well understood.[22] However, recent simulations have shown that these two effects are unimportant for glass transition physics.[23–26] The third difference being the polydispersity of the samples which eventually frustrates the system from crystallization and shifts the phase transition points to a higher Φs.[27–29] In addition, recent observations of spontaneous crystallization of colloidal glass in microgravity[30] has led to some controversy about the effect of gravity on colloidal glass transition phenomena. However, given the fact that predictions from gravity free simulations are in excellent agreement with colloidal experiments, it is plausible that gravity does not have any role in the the observations of colloidal glasses. It is worthwhile to mention that whether or not hard sphere show a glass transition, there is clearly a change in the nucleation mechanism in the vicinity of glass transition.[31]

1.4 Colloids as Model Systems to Study Glass Transition

1.4.1 Colloidal Suspensions

The word colloid is derived from the Greek word "kolla" (glue) and "eidos" (appearance) and was coined by Thomas Graham, a Scottish chemist in 1861. According to Britannica Online Encyclopedia, "A colloid is a substance microscopically dispersed throughout another substance". Depending upon the state of the dispersed phase/first substance and dispersed media/second substance, colloids are classified into various categories like, suspension/dispersion - solid particles in a liquid, foams - gas bubbles in liquid/solid medium, emulsion - liquid droplets in an immiscible liquid and so on. The main focus here would be on colloidal suspensions (Figure 1.6) where the size of the particles suspended in the liquid is of the order of microns. Examples of colloidal suspensions are, fat particles suspended in water (milk), metal particles (lead etc.) suspended in motor oil, coloured pigments suspended in paints etc. Colloidal particles are stabilized by electrostatic or steric repulsion. In the for-

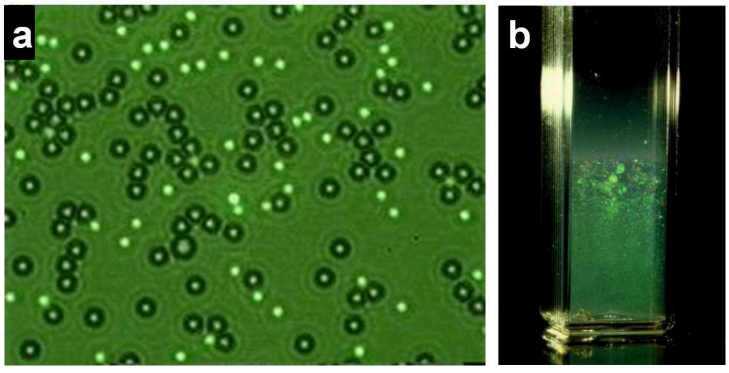

Figure 1.6: (a) Colloidal suspension (b) Spherical colloidal particles in a refractive index matched solvent. Hence they are not visible in isotropic phase but they show Bragg scattering in the crystalline phase at the bottom. Adopted from.[33]

mer case, the electric charges on the surface of particles stabilize it e.g. polystyrene

(PS) particles in water. Stability of these colloids are described by DLVO (Derjaguin and Landau, Verwey and Overbeek) theory[32] which takes into account the double layer formation of counter-ions around colloidal particles. In the latter case, polymeric molecules either chemically attached or adsorbed on particles stabilize it[32] e.g. polymethyl methaacrylate (PMMA) particles in oil. Here, the polymer chain dimensions are larger than the van der Waals attraction range.[32] The size of colloidal particles are big enough that their dynamics can be studied using the laws of classical mechanics. However, they are small enough that thermal fluctuations of the suspensions give Brownian motion to the particles (Figure 1.6). The diffusion time, τ_D, of the these micron sized particles is of the order 1 ms to 1 s and they can be seen using an optical microscope and hence are good models (Figure 1.6) to study phenomena inaccessible in atomic experiments such as nucleation and growth,[34–36] grain boundary dynamics in polycrystals,[37,38] packing of particles in micron sized confined geometries,[39,40] superheating,[41] self assembly[42,43] etc. Colloids have numerous applications in everyday life and industrial processes e.g tooth paste, shaving cream, milk, liquid and mineral purification, oil recovery and processing etc.

Historically, it was in late 1970s, experiments demonstrated the resemblance of structure in colloids and atomic systems.[44,45] This heralded the use of colloids as a model system to study phase transitions. It was Lindsay and Chaikin in 1982 who observed a glassy phase in a binary system which was later confirmed by simulations.[46] In 1986-87, Pusey and van Megen showed the glass transition in sterically stabilized, hard-sphere PMMA colloidal particles.[47–49]

1.4.2 Colloidal Glass Transition and Glasses

In a seminal work, Pusey *et. al.*[47,48] used 305 nm of sterically stabilized PMMA spherical colloidal particles and realized phases as function of Φ as shown in Figure 1.7. For the first time, using dynamic light scattering (DLS) techniques, they

Figure 1.7: Nearly hard spheres colloidal suspension, 4 days after tumbling. States of the suspensions from left, first - fluid; next three - liquid-crystal coexistence; next two - homogeneous crystal; 7^{th} - heterogeneous crystal; last two - glass. Bragg scattering can be observed in crystalline samples. The last sample did not crystallize even after several months. Adopted from.[47]

showed that the glass transition at $\Phi_g = 0.565$.[48] In DLS, the temporal fluctuations of scattered light, at a given wave vector $\mathbf{q}$, have information about the dynamics of the system. The normalized time correlation of the scattered light for given $\mathbf{q}$, $g^{(2)}(\mathbf{q}, t)$ yields the $F_s(q, t)$,

$$g^{(2)}(\mathbf{q}, t) = 1 + [\tfrac{cF_s(\mathbf{q},t)}{S(q)}]^2$$

where c is an instrument constant. The typical decay behaviour of $F_s(q, t)$ adopted from Pusey *et. al.*[48]is shown in Figure 1.8. While at low Φs, the decay is exponential; for intermediate Φs, the decay is non-exponential (Figure 1.8). For high Φs, $\Phi >$ 0.565, only partial decay is observed in $F_s(q, t)$ (Figure 1.8) and the systems were found to be glassy. The Φ at which $F_s(q, t)$ decayed only partially was termed as glass transition volume fraction $\Phi_g = 0.565$.[48]

In a major breakthrough experiment, Weeks *et al*[50] and Kegel *et al.*[51] used micron sized colloidal particles to investigate the structure and dynamics of super-cooled liquid and glasses at single particle resolution. The particle dynamics was quantified using the mean squared displacements (MSD).

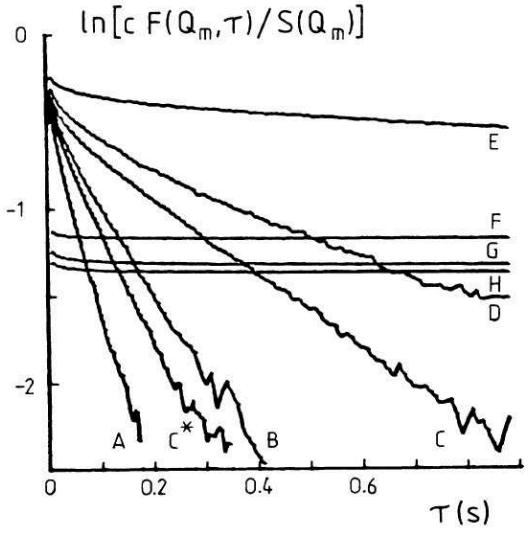

Figure 1.8: Semilogarithmic plot of $F_s(q,t)$ with delay time τ for different samples. A - fluid; C* - fluid-fluid coexistence; B, C, D - fluid-crystal coexistence; E, F - crystals; G, H, I, J - glass. Adopted from.[48]

$$\langle \Delta r^2 \rangle = \frac{1}{N} \langle \sum_{j=1}^{N} [(x_j(t+t_0) - x_j(t))^2 + (y_j(t+t_0) - y_j(t))^2] \rangle$$

Here N is the total number of particles, $x_j(t)$ and $y_j(t)$ are the coordinates of j^{th} particle, t_0 is the lag time, $\langle\rangle$ indicates average over all particles and all initial time t for a particular t_0. MSD as a function of Φ is shown in Figure 1.9 A. At low Φ, the dynamics is diffusive (Figure 1.9 A).

$$\langle \Delta r^2 \rangle = 4D\Delta t$$

where D is the diffusion coefficient of particles. D of particles depends upon the solvent's η and T through the Stokes-Einstein-Sutherland equation[52,53] as,

$$D = \frac{k_B T}{6\pi\eta r}$$

As Φ increases, MSD starts developing a plateau at intermediate time and the dynamics becomes sub-diffusive,[50]

$$\langle \Delta r^2 \rangle = 4D(\Delta t)^{\nu} \text{ where } \nu < 1.$$

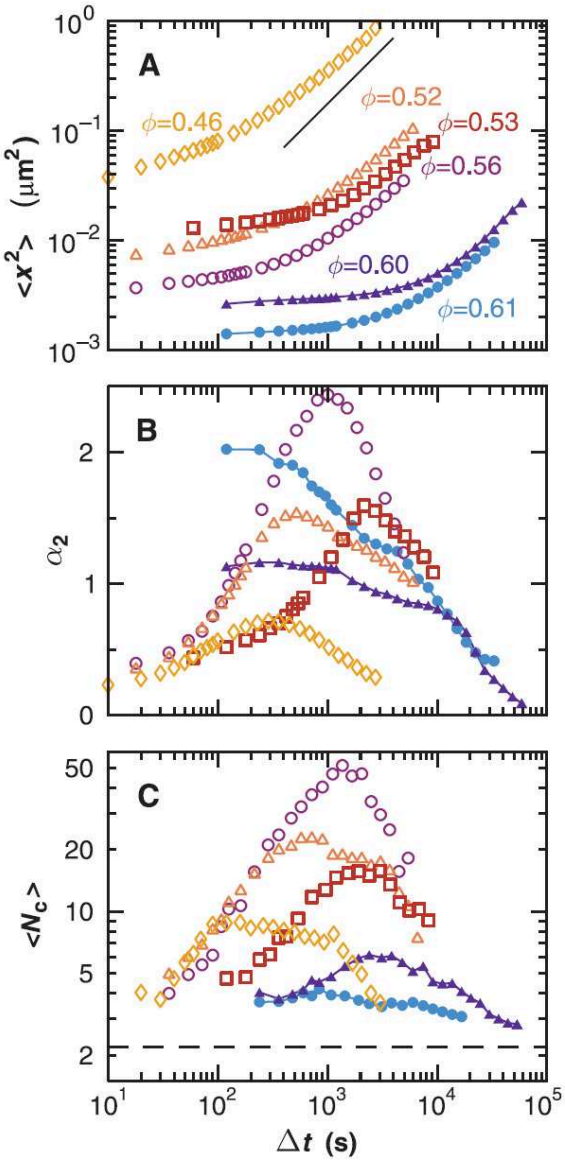

Figure 1.9: (A) $\langle \Delta r^2 \rangle$ at various volume fraction Φ as indicated in the plot. The solid line has slope 1. (B) The non-Gaussian parameter $\alpha_2(t)$ and (C) the particle avergared cluster size of fast particles, $\langle N_c \rangle$ with time. The Φs in (B) and (C) are color coded as in (A). The dashed line shows the expected result for random distribution of fast particles. Adopted from.[50]

Here, ν is the diffusion exponent. This plateau region indicates caging of particles by their neighbours which become stronger with Φ. These observations are in agreement with MCT.[15,17] At the characteristic time $t = t^*$, an upturn in MSD is observed which indicates cage relaxation. The upturn in MSD signifies non-Gaussian particle displacements and are best quantified using the non-Gaussian parameter, $\alpha_2(t)$,[50]

$$\alpha_2(t) = \frac{\langle \Delta r(t)^4 \rangle}{2\langle \Delta r(t)^2 \rangle} - 1$$

where $\Delta r(t)$ is the displacements of particles over t. Since for any Gaussian process all higher order moments can be expressed in terms of $\langle \Delta r^2(t) \rangle$, $\alpha_2(t) = 0$ for diffusive dynamics. However, for supercooled liquids, $\alpha_2(t)$ show a maximum in the vicinity of t^* due to cage rearrangements (Figure 1.9 B). For $\Phi \geq 0.58$, the peaks were broader and not as high as observed at lower Φs[50] (Figure 1.9 B). This sharp change in behaviour of $\alpha_2(t)$ was identified as glass transition with $\Phi_g = 0.58 \pm 0.01$[50] which was in agreement with the previous works.[47,48,54]

The non-Gaussian particle dynamics at t^* are best reflected in the probability distribution of displacements, $(P(\Delta r(t)))$, over t^* as shown in Figure 1.10. The tail of the distribution is non-Gaussian signifying that a fraction of total particles have higher nobilities as compared to their neighbours (Figure 1.10). The dynamics over t^* are thus heterogeneous (Figure 1.11). It was also observed that these most-mobile particles were spatially clustered and varied with time.[50] For the first time, these dynamical heterogeneities, believed to be pathways of structural relaxations in supercooled liquid,[8] were observed in an experiment[50] (Figure 1.11). Further, the particle averaged cluster size of fast particles, $\langle N_c \rangle$, defined as,[55]

$$\langle N_c \rangle = \frac{\sum_n n^2 P(n)}{\sum_n n P(n)}$$

followed the same trend with time as $\alpha_2(t)$ (Figure 1.9 C). Here $P(n)$, is the probability of finding a cluster of size n. $\langle N_c \rangle$ was observed to be highest at t^*[50] (Figure 1.9 C). Further, $\langle N_c \rangle$ increases on approaching Φ_g and decreases drastically beyond

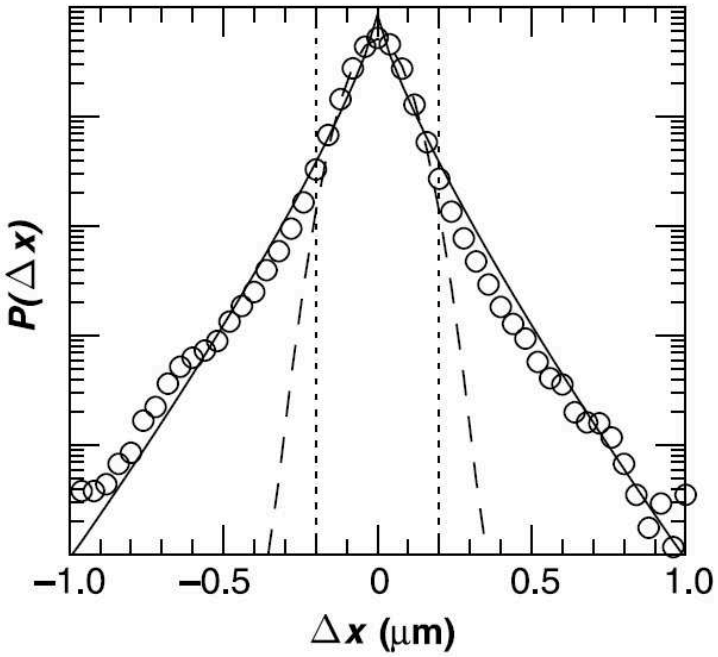

Figure 1.10: The probability distribution of displacements, $(P(\Delta r(t)))$, over t^* for $\Phi = 0.56$. The dashed line is best fit Gaussian, the solid line is a stretched exponential fit to the tails of the distribution. The particles within dotted lines are slowest 95%. Adopted from.[50]

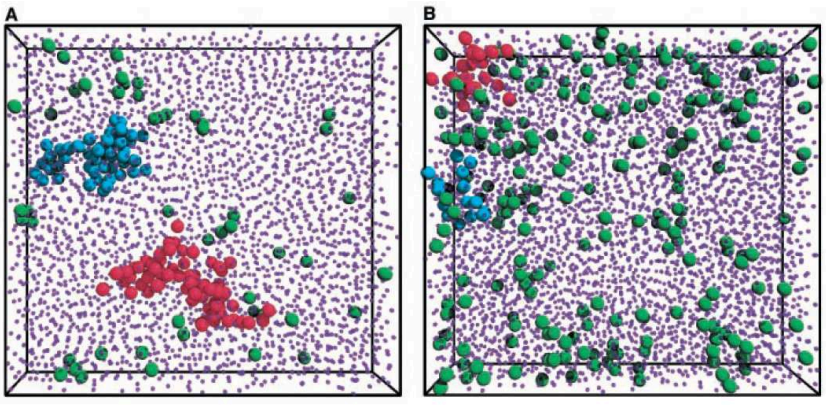

Figure 1.11: Spatial distribution of clusters fastest particles (large spheres). For clarity, the slowest (95% of the particles are shown as small spheres in the background. (A) Supercooled liquid at $\Phi = 0.56$. (B) Glass at $\Phi = 0.61$. Particles belonging to the same clusters are shown in same color. Adopted from.[50]

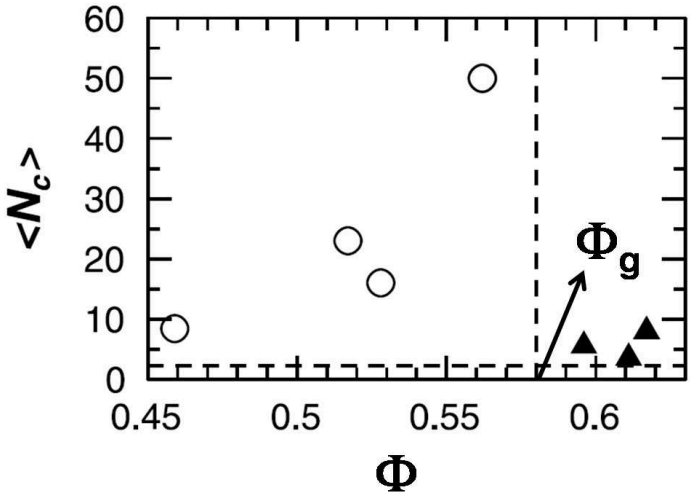

Figure 1.12: The variation of $\langle N_c \rangle$ with Φ. The dashed horizontal line indicates $\langle N_c \rangle$ for random distribution of fast particles. The vertical dashed line represents Φ_g. Adopted from.[50]

$\Phi \approx 0.58 = \Phi_g$ (Figure 1.12).[50] The dramatic change in the behaviour of $\langle N_c \rangle$, further confirmed that $\Phi_g = 0.58 \pm 0.01$. The decrease in $\langle N_c \rangle$ beyond Φ_g was attributed to much slower relaxation i.e. t^* in the vicinity of Φ_g corresponds to β-relaxation and not to cage relaxation.[50]

So far, we have seen that spherical colloids with purely repulsive interactions give a microscopic insight into the physics of glass transitions. Now, we will discuss on the change in particle interaction potentials and its influence on the glass transition physics.[31,56–65]

1.5 Attractive Glasses

When the interaction potential between the particles is changed from repulsive to attractive, MCT predicted the existence of yet another glass - the attractive glass.[61,66,67] The typical phase diagram, in (T, Φ) plane, as predicted by MCT,[66] is shown in Figure 1.13. MCT predicted two lines of transition from liquid to glass. While one of them extended to high temperature and asymptotically approached

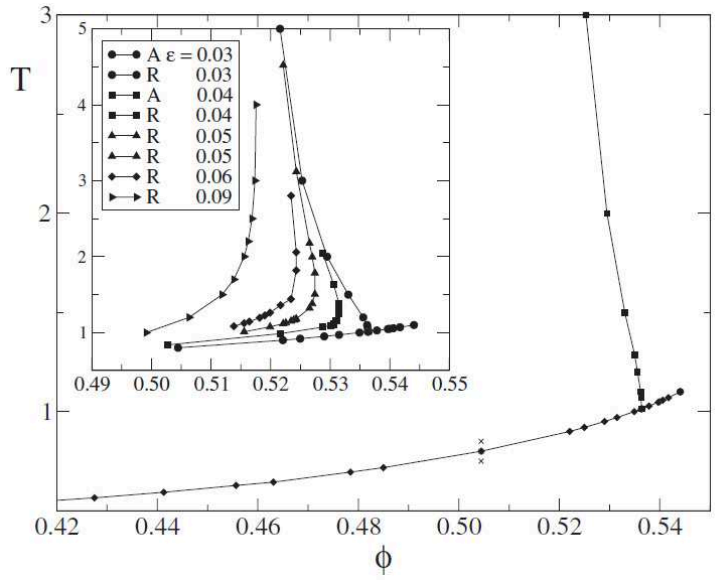

Figure 1.13: Phase diagram for a square-well system with square well of relative width $\varepsilon = 0.03$. The inset shows the phase diagram, where AGL and RGL are shown at various ε. Adopted from.[66]

the repulsive glass transition Φ, the other line originated at some finite value of attractive potential and was almost parallel to the Φ- axis at lower temperature[61,66] (Figure 1.13). While the former was called as repulsive glass line (RGL), the latter was called as attractive glass line (AGL). As we move down the T-axis at a fixed Φ, the transition line moves towards higher Φ (RGL) and comes back to a lower Φ (AGL) with increasing attraction strengths (Figure 1.13). This is termed as reentrant in glassy dynamics i.e. at a fixed temperature greater than the repulsive glass transition temperature (RG T_g), a repulsive glass (RG) melts to an ergodic fluid and forms a novel glass - attractive glass (AG) - at even higher interaction strengths (Figure 1.13).[61,66] The reasons for emergence of different glasses was attributed to two competing length scales set by attractive and repulsive potential. While the dynamics in RG is dominated by cage relaxations, in AG, bonding between the particles dictates the dynamics. Further, the shift of RGL to higher Φ depends on the relative width of attractive potential to repulsive potential, ε, (inset

to Figure 1.13).[61,66] The endpoint of the AGL is a higher order glass transition point (called A_3 point), beyond which the distinction between AG and RG vanishes.[61,66] This implies that the length scale set by the range of the interaction potential is comparable to how much a particle can move within a cage.

The above MCT predictions were realized experimentally by, Pham *et. al.*[31] and Eckert *et. al.*[57] who independently used short-range depletion interaction[68] to introduce an attraction between the colloidal particles. The sizes of the depletant particles (r_g) are smaller than colloidal particles (R) i.e. $\frac{r_g}{R} = \varepsilon < 1$. As shown in Figure 1.14, the centres of the small polymer particles cannot enter within an excluded volume (determined by r_g) around large spherical colloid.

$$U_{dep} = -\frac{R}{r_g}\phi_{poly}k_BT$$

where symbols have usual meaning. When the big colloidal particles come together, their excluded volume overlaps and subsequently free up an equivalent volume for the small polymer particles. This increases the entropy of the depletant particles and hence induces an effective attraction between the large colloids (Figure 1.14). The strength and range of this attractive interaction can be tuned by changing the concentration, ϕ_{poly} and r_g, respectively.

Hence, for a narrow range of Φs with $\Phi > \Phi_g$ as function of increasing attraction strength, a RG (sample A in Figure 1.15) melts to an ergodic fluid (sample B in Figure 1.15) at intermediate c_ps and forms a AG (sample C, D and E in Figure 1.15) at higher c_p which is reflected in decay behaviour of $F_s(q,t)$ (Figure 1.15).[31] At low and high attraction strengths, $F_s(q,t)$ showed a two-step relaxation and only a partial decay even at long times. Whereas, at intermediate attraction strengths, $F_s(q,t)$ decayed completely with a shift in Φ_g to higher Φs.[31,57] The larger plateau value at long times for samples C, D and E implies a relatively stronger freezing-in of long-wavelength collective density fluctuations (Figure 1.15).[31] Though the short-time dynamics in attractive glasses is dominated by bond breaking, recent

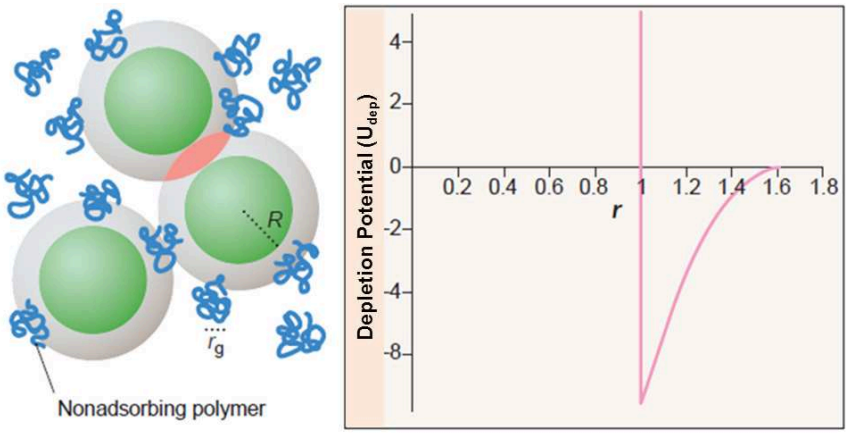

Figure 1.14: Depletion attraction. Left - Schematic of colloid-polymer suspension. Excluded volume (light gray) around each colloidal particle, polymer molecules with radius of gyration, r_g and red region represent the overlap of excluded volume leading to attraction between particles. Right - Schematic of depletion induced attractive potential. Adopted from.[69]

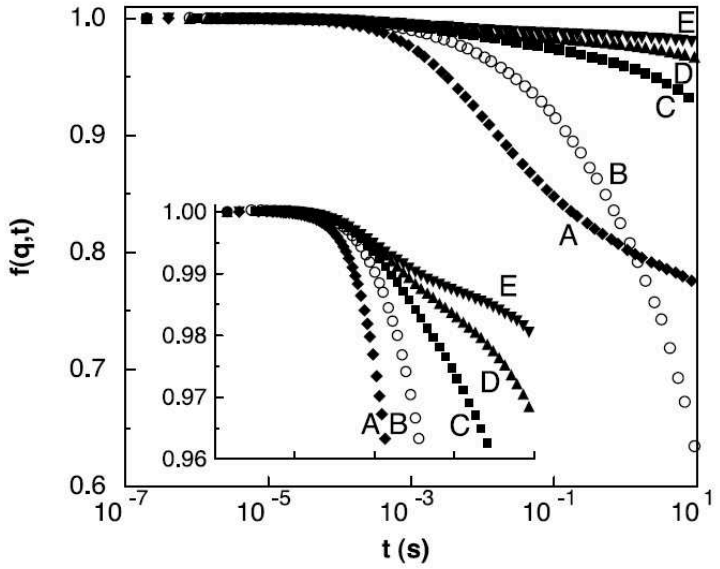

Figure 1.15: $F_s(q,t)$ as a function of time, t, at various depletion concentration at a fixed Φ. sample A - repulsive glass, sample B - ergodic fluid, sample C, D and E - attractive glass. Adopted from.[31]

simulations have shown that analogous to repulsive glasses, structural relaxation at long times is still governed by cage rearrangements.[70] Further, based on the decay behaviour of $F_s(q, t_\infty)$, complete phase diagram has been been shown below (Figure 1.16).[31] Here t_∞, represents experimental time duration.

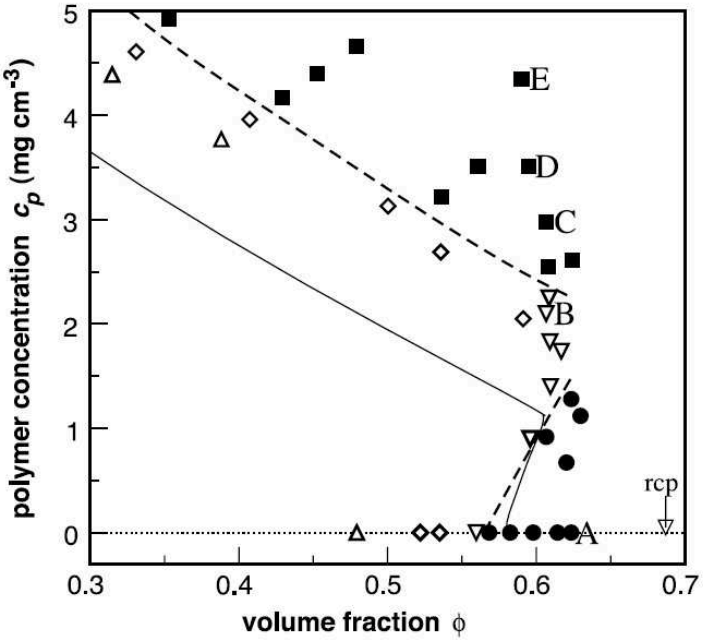

Figure 1.16: Phase diagram of colloid-polymer mixture in (c_p, Φ) plane. Open symbols represent thermally equilibrated samples: fluids (triangles), fluid-crystal coexistence (diamonds), fully crystalline (inverted triangles). Solid symbols represents non-equilibrated samples: repulsion driven glass (circles), attraction driven glass (squares). dashed curves are guide to the eye for observed glass transition. Solid lines are MCT predicted glass transition lines. Adopted from.[31]

1.6 Shape Anisotropy and the Glass Transition

Anisotropy in shape and/or interactions is a feature of many molecular systems.[71] In the recent past, there have been significant efforts by the colloid community to synthesize colloids of different shapes i.e. ellipsoids,[72] rods,[73] polygons (tetrahedrons, pentagons),[74,75] cuboids[76]etc. Further, particle shape strongly influences

their packing[4] as Donev *et. al.*[77] have shown that oblate ellipsoids with aspect ratio, α, close to M&M candies can pack beyond the random closed packing (RCP) of spheres ($\Phi_{RCP} = 0.64$). They attribute the attainment of the higher packing to the extra degree of freedom (DOF) available to ellipsoids as compared to spheres. Inspite of the fact that packing and glass transition physics are closely related, it is only recently that the role of shape anisotropy in the physics of glass transitions has been probed. The first tentative phase diagram for ellipsoids, the simplest deviation from a spherical particles, as function of aspect ratio ($\alpha = l/w$) was proposed by Frenkel *et. al.*[78] in 1984. Here l and w are major and minor axes of ellipsoid. Later, using molecular mode coupling theory (MMCT)[79–81] and Monte-Carlo simulations,[82] a rich and complex phase diagram has been proposed for ellipsoids (Figure 1.17). MMCT predicts that with increasing α, the glass transition for prolate ellipsoids is primarily driven by the orientational degree of freedom (DOF).[80] Further, it predicts a two-step glass transition for $\alpha \geq 2.5$, with formation of nematic domains where interdomain orientational freezing precedes the intradomain translational freezing and a single conventional glass transition for short α ($\alpha \leq 2.5$) with isotropic structure.[80] In 2003, Cang *et al.*[84] showed that the 5-CB liquid crystalline molecule has two glass transition temperatures. As predicted by MMCT,[80] they alluded the first glass transition temperature T_{CH} to the freezing of the local nematic order associated with the psuedonematic domains and the second T_{CL} to the freezing of intradomain dynamics of psuedonematic domains. Later, using micron sized prolate colloidal ellipsoids of $\alpha = 6$ in quasi 2-dimension (2D), Zheng *et. al.*[85] showed psuedonematic ordering with branch like structures. The translational and orientational dynamics were quantified using $F_s(q,t)$ and orientational correlation function, $L_n(t)$, respectively where

$$L_n(t) = \frac{1}{N}\langle \sum_{j=1}^{N} P_n(\cos(\theta_j(t+t_0) - \theta_j(t)))\rangle$$

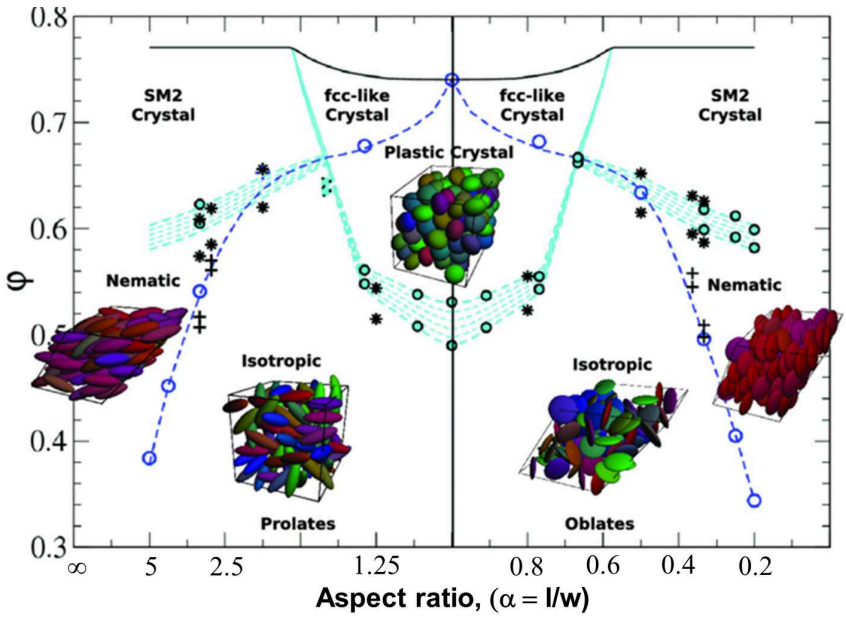

Figure 1.17: Phase diagram of uniaxial hard ellipsoids in (Φ, α) plane. Solid symbols corresponds to fluid-solid transition, hollow symbol corresponds to isotropic-nematic transition. The black (dark) line is maximum achievable density.[83] Cyan (light gray) dashed lines and blue (dark) dashed lines are guides to the eye which join the fluid-solid and isotropic-nematic transitions, respectively. The cyan (light gray) solid lines indicate fcc-SM2 transitions.[79] Black (dark) plus symbols (isotropic-nematic) and asterisks (nematic-solid) are taken from the.[78] The inserted snapshots are placed according to the phase diagram region. Particles are colored according to their orientations by setting red, blue, and green to given orthogonal directions, and using a linear combination for intermediate cases. Adopted from.[82]

Here, N is the total number of particles, $\theta_j(t)$ is the orientation of the j^{th} ellipsoid at time t, t_0 is the lag time, $P_n(\cos(\theta))$ is the n^{th} order Legendre polynomial and $\langle\rangle$ denotes the time averaging. The glass transition area fraction ϕ_g for both translational and orientational degree of freedom (DOF) was estimated using MCT scaling arguments.[85] Consistent with MCT predictions, ${\tau_\alpha}^{-1/\gamma}$ was found to be linear in ϕ for both translational and orientational DOF (Figure 1.18) and yielded orientational glass transition area fraction $\phi_g^R = 0.72 \pm 0.01$ and translational glass transition area fraction $\phi_g^T = 0.79 \pm 0.01$ (Figure 1.18) which was in qualitative agreement with experiments on liquid crystals,[84] molecular mode coupling theory (MMCT) predictions and computer simulations[80,86,87] Further, in excellent agree-

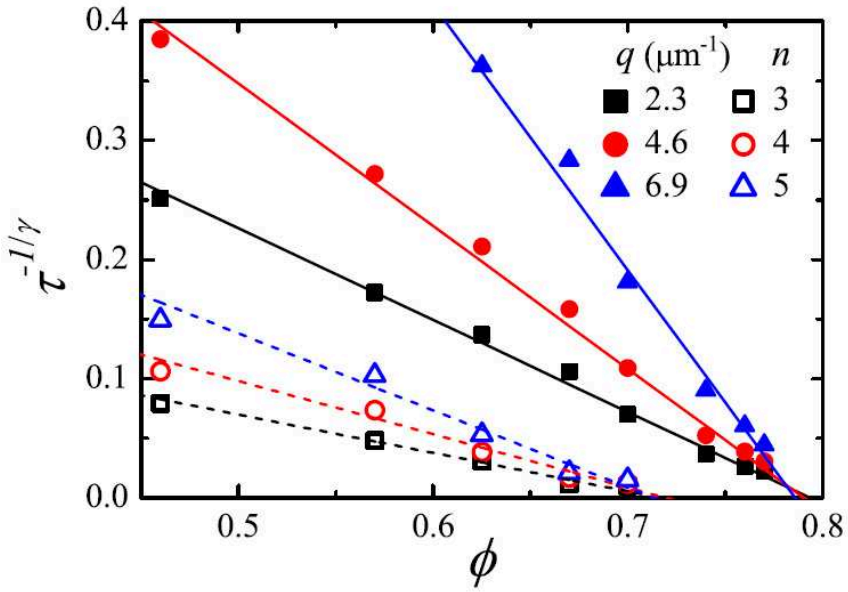

Figure 1.18: ${\tau_\alpha}^{-1/\gamma}$ *vs* ϕ. Open and solid symbols correspond to orientational and translational DOF, respectively. Dashed and solid lines are linear fits to the data. Adopted from.[85]

ment with Cang *et. al.*,[84] most of translationally most-mobile particles were within the psuedonematic domains and most of rotationally most-mobile particles were at the domain boundaries (Figure 1.19).[85] In addition, they showed that the intermediate orientational glass regime which lies between ϕ_g^R and ϕ_g^T increases as α of

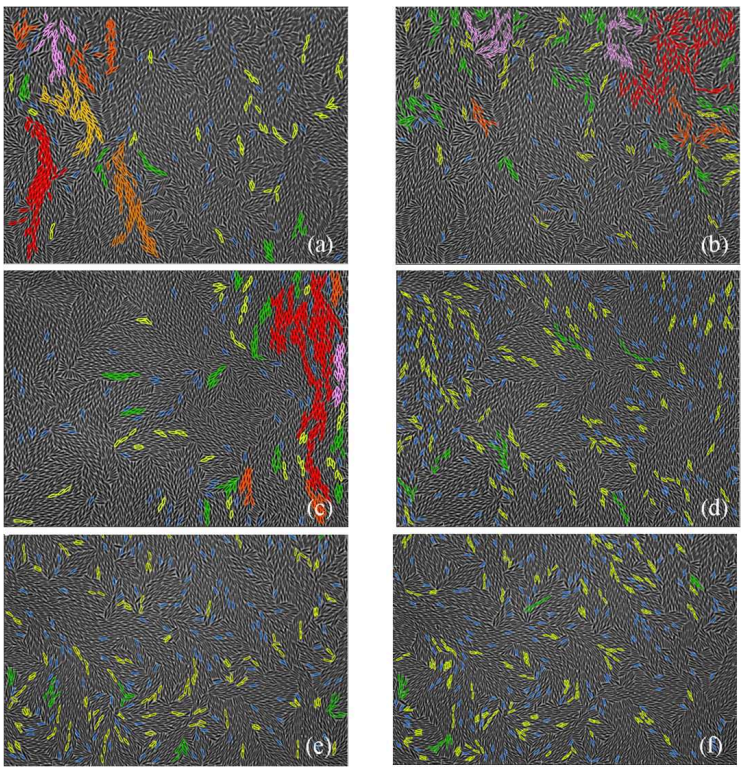

Figure 1.19: The spatial distribution of rotational (b, d, f) and translational (a, c, e) most-mobile particles of the system. (a), (b) at $\phi = 0.70$ (supercooled liquid); (c), (d) at $\phi = 0.77$ (orientational glass); (e), (f) at $\phi = 0.81$ (glass). ellipsoids in same cluster have same color. Adopted from.[85]

ellipsoids increase.[85]

1.7 Motivation for the Present Work

As discussed, colloidal ellipsoids of $\alpha = 6$ in 2D yielded a two-step glass transition.[85] Further, in concordance with the fact that packing of the ellipsoids strongly depends on their α,[4] molecular mode coupling theory (MMCT) predicts that ellipsoids with $\alpha < 2.5$ in 3D should show a single glass transition.[80] Nevertheless, so far, even in 2D there is no experimental evidence for the same. Hence, it would be interesting to investigate the self-assembly and structural relaxation in supercooled liquid and glasses of short colloidal ellipsoids.

Most importantly, due to the presence of two radii of curvatures, the depletion interactions in ellipsoids lead to anisotropic interactions[88] where lateral alignment of ellipsoids would be preferred as compared to tip-to-tip alignment (Figure 1.20). However, the role of interaction anisotropy in the physics of glass transition is yet

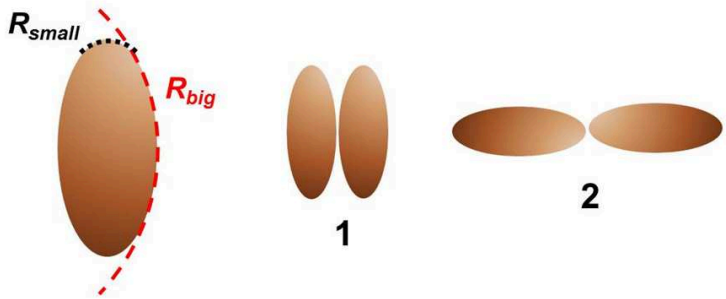

Figure 1.20: Two radii of curvature for the ellipsoids; R_{big} and R_{small}. When depletion attraction is turned on, due to anisotropy configuration 1 is preferred over 2.

to be probed by experiments, simulations and theory. Hence, it would also be fascinating to investigate the influence of asymmetric interaction potential on reentrant glass dynamics. We have, in the present work, explored the complete phase diagram of colloidal ellipsoids of $\alpha = 2.1$ in (U, ϕ) plane where U is the angle averaged

interaction potential for a given c_p.

Bibliography

[1] C.A. Angell, Science **267**, 1924 (1995); A.L. Greer, *ibid.* **267**, 1947 (1995); B. Frick and D. Richter, *ibid.* **267**, 1939 (1995); F.H. Stillinger, *ibid.* **267**, 1935 (1995); J.I. Brauman, *ibid.* **267**, 1887 (1995).

[2] L. Berthier and G. Biroli, Rev. Mod. Phys. **83**, 587 (2011) and references therein.

[3] K.A. Dawson, Curr. Opin. Colloid Interf. Sci **7**, 218 (2002) and references therein.

[4] S. Torquato and F.H. Stillinger, Rev. Mod. Phys. **82**, 2633 (2010) and references therein.

[5] M. H. Cohen and D.J. Turnbell, J. Chem. Phys. **31**, 1164 (1959).

[6] D.J. Turnbell and M. H. Cohen, J. Chem. Phys. **34**, 120 (1961).

[7] J. H. Gibbs and E. A. Di Marzio, J. Chem. Phys. **28**, 373 (1958).

[8] G. Adam and J.H. Gibbs, J. Chem. Phys. **43**, 139 (1965).

[9] R.G. Palmer, D.L. Stein, E. Abrahams, and P.W. Anderson, Phys. Rev. Lett. **53**, 958 (1984).

[10] G.H. Fredrickson and H.C. Andersen, Phys. Rev. Lett. **53**, 1244 (1984).

[11] U. Bengtzelius, W. Gotze, and A. Sjolander, J Phys. C **17**, 5915 (1984).

[12] E. Leuthesser, Phys. Rev. A **29**, 2765 (1984).

[13] Walter Kob."The mode-coupling theory of the glass transition." ACS Symposium Series. Vol. **676**. American Chemical Society (1997).

[14] P. G. Debenedetti, and F. H. Stillinger, Nature **410**, 259 (2001).

[15] W. Gotze and L. Sjogren, Rep. Prog. Phys. **55**, 241 (1992).

[16] W. Gotze, J. Phys.: Condens. Matter **2**, 8485 (1990).

[17] W. Kob and H. C. Andersen, Phys. Rev. Lett. **73**, 1376 (1994).

[18] T. Kob and W. Gleim, Eur. Phys. J. B **13**, 83 (2000).

[19] http://weitzlab.seas.harvard.edu/research/jensen-katharine.html

[20] E. Bartsch, Curr. Opin. Colloid Interface Sci **3**, 577 (1998).

[21] K. S. Schweizer and G. Yatsenko, J. Chem. Phys. **127**, 164505 (2007).

[22] E. Di Cola, A. Moussaid, M. Sztucki, T. Narayanan, and E. Zaccarelli, J. Chem. Phys. **131**, 144903 (2009).

[23] T. Gleim, W. Kob, and K. Binder, Phys. Rev. Lett. **81**, 4404 (1998).

[24] M. Tokuyama, H. Yamazaki, and Y. Terada, Phys. Rev. E **67**, 779 (2003).

[25] L. Berthier, G. Biroli, J. P. Bauchaud, W. Kob, K. Miyazaki, and D.R. Reichman, J. Chem. Phys. **128**, 164517 (2007).

[26] A. M. Puertas, J. Phys.: Condens. Matter **22**, 104121 (2010).

[27] P. G. Bolhuis and D. A. Kofke, Phys. Rev. E **54**, 634 (1996).

[28] M. Fasolo and P. Sollich, Phys. Rev. Lett. **91**, 068301 (2003).

[29] P. Sollich and N. B. Wilding, Phys. Rev. Lett. **104**, 118302 (2010).

[30] J. Zhu, M. Li, R. Rogers, W. Meyer, R. H. Ottewill, STS-73 Space Shuttle Crew, W.B. Russel, and P. M. Chaikin, Nature **387** , 883 (1997).

[31] K.N. Pham, A.M. Puertas, J. Bergenholtz, S.U. Egelhaaf, A. Moussaid, P.N. Pusey, A.B. Schofield, M.E. Cates, M. Fuchs, and W.C.K. Poon, Science **296**, 104 (2002).

[32] J. N. Israelachvili, Intermolecular and surface forces: revised third edition. Academic press, 2011.

[33] P. Pfleiderer, "Crystal Phases and Glassy Dynamics in Monodisperse Hard Ellipsoids." PhD diss., 2008.

[34] U. Gasser, E. R. Weeks, A. Schofield, P. N. Pusey, and D. A. Weitz, Science **292**, 258 (2001).

[35] Z. Cheng, W. B. Russel, and P. M. Chaikin, Nature **401**, 893 (1999).

[36] R. Ganapathy, M. R. Buckley, S. Gerbode and I. Cohen, Science **327**, 445 (2010).

[37] H. K. Nagamanasa, S. Gokhale, R. Ganapathy, and A. K. Sood, Proc. Nat. Acad. Sci. **108**, 11323 (2011).

[38] S. Gokhale, H. K. Nagamanasa, V. Santhosh, A. K. Sood, and R. Ganapathy. Proc. Nat. Acad. Sci. **109**, 20314 (2012).

[39] V. N. Manoharan, M. T. Elsesser, and D. J. Pine, Science **301**, 483 (2003).

[40] V. N. Manoharan and D. J. Pine, MRS Bulletin **29** 91 (2004) and refrences therein.

[41] Z. Wang, F. Wang, Y Peng, Z. Zheng, and Yilong Han, Science **338**, 87 (2012).

[42] S. C. Glotzer, M. J. Solomon, and N. A. Kotov, AIChE Journal **50**, 2978 (2004).

[43] A. D. Dinsmore, J. C. Crocker, and A. G. Yodh, Current Opin. in colloid & interface science **3**, 5 (1998).

[44] R. Hastings, J. Chem. Phys. **68**, 675 (1978).

[45] C. A. Murray and D. H. Van Winkle, Phys. Rev. Lett. **58**, 1200 (1987).

[46] H. M. Lindsay and P. M. Chaikin, J. Chem. Phys. **76**, 3774 (1982).

[47] P.N. Pusey and W.van Megan, Nature **320**, 340 (1986).

[48] P. N. Pusey and W. van Megen, Phys. Rev. Lett. **59**, 2083 (1987).

[49] W. van Megan, S. M. Underwood, Phys. Rev. E **47**, 248 (1993).

[50] E.R. Weeks, J.C. Crocker, A.C. Levitt, A. Schofield, and D.A. Weitz, Science **287**, 627 (2000).

[51] W.K. Kegel and A. van Blaaderen, Science **287**, 690 (2000).

[52] W. Sutherland, Phil. Mag. **9**, 781 (1905).

[53] A. Einstein, Ann . Phys., Lpz. **17**, 549 (1905).

[54] A. Kasper, E. Bartsch, and H. Sillescu, Langmuir **14**, 5004 (1998).

[55] S.C. Glotzer, J. Non-Cryst. Solids **274**, 342 (2000).

[56] J. Mattsson, H.M. Wyss, A. Fernandez-Nieves, K. Miyazaki, Z. Hu, D.A. Reichman, and D.A. Weitz, Nature **462**, 82 (2009).

[57] T. Eckert and E. Bartsch, Phys. Rev. Lett. **89**, 125701 (2002).

[58] A. Latka, Y. Han, A.M. Alsayed, A.B. Schofield, A.G. Yodh, and P. Habdas, Europhys. Lett. **86**, 58001 (2009).

[59] L.J. Kaufman and D.A. Weitz, J. Chem. Phys. **125**, 074716 (2006).

[60] N.B. Simeonova, R.P.A. Dullens, D.G.A.L. Aarts, V.W.A. de Villeneuve, H.N.W. Lekkerkerker, and W.K. Kegel, Phys. Rev. E **73**, 041401 (2006).

[61] K. Dawson, G. Foffi, M. Fuchs, W. Gotze, F. Sciortino, M. Sperl, P. Tartaglia, Th. Voigtmann, and E. Zaccarelli, Phys. Rev. E **63**, 011401 (2000).

[62] R. C. Kramb, R. Zhang, K. S. Schweizer, and C. F. Zukoski, Phys. Rev. Lett. **105**, 055702 (2010).

[63] Q. Chen, S.C. Bae, and S. Granick, Nature **469**, 381 (2011).

[64] D.J. Kraft, R. Ni, F. Smallenburg, M.Hermes, K. Yoon, D.A. Weitz, A. van Blaaderen, J. Groenewold, M. Dijkstra, and W.K. Kegel, Proc. Nat. Acad. Sci. **109**, 10787 (2012).

[65] A. Yethiraj and A. van Blaaderen, Nature **421**, 513 (2003).

[66] K.A. Dawson, G. Foffi, F. Sciortino, P. Tartaglia, and E. Zaccarelli, J. Phys.: Condens. Matter **13**, 9113 (2001).

[67] A.M. Puertas, M. Fuchs, and M.E. Cates, Phys. Rev. Lett. **88**, 098301 (2002).

[68] S. Asakura and F. Oosawa, J. Chem. Phys. **22**, 1255 (1954).

[69] W. Poon, Science **304**, 830 (2004).

[70] E. Zaccarelli and W.C.K. Poon, Proc. Nat. Acad. Sci. **106**, 15203 (2009).

[71] E. R. Weeks, Physics **4** ,61 (2011).

[72] C.C. Ho, A. Keller, J.A. Odell, and R.H. Ottewill, Colloid Polym. Sci **271**, 469 (1993).

[73] A. Kuijk, A. van Blaaderen, and A. Imhof, J. Am. Chem. Soc. **133**, 2346 (2011).

[74] Y. Wang, Y. Wang, D. R. Breed, V. N. Manoharan, L. Feng, A. D. Hollingsworth, M. Weck, and D. J. Pine, Nature **491**, 51 (2012).

[75] K. Zhao and T.G. Mason, Phys. Rev. Lett. **103,** 208302 (2009).

[76] L. Rossi, S. Sacanna, W. T. M. Irvine, P. M. Chaikin, D. J. Pine, and A. P. Philipse, Soft Matter **7**, 4139 (2011).

[77] A. Donev, I. Cisse, D. Sachs, E. A. Variano, F. H. Stillinger, R. Connelly, S. Torquato, and P. M. Chaikin, Science **303**, 990 (2004).

[78] D. Frenkel and B. M. Mulder, Mol. Phys. **55**, 1171 (1985).

[79] M. Radu, P. Pfleiderer, and T. Schilling, J. Chem. Phys. **131**, 164513 (2009).

[80] M. Letz, R. Schilling, and A. Latz, Phys. Rev. E **62**, 5173 (2000).

[81] P. Pfleiderer and T. Schilling, Phys. Rev. E **75**, 020402 (2007).

[82] G. Odrizola, J. Chem. Phys. **136**, 134505 (2012).

[83] A. Donev, F. H. Stillinger, P. M. Chaikin, and S. Torquato, Phys. Rev. Lett. **92**, 255506 (2004)

[84] H. Cang, J. Li, V.N. Novikov, and M.D. Fayer, J. Chem. Phys. **119**, 10421 (2003).

[85] Z. Zheng, F. Wang, and Y. Han, Phys. Rev. Lett. **107**, 065702 (2011).

[86] C. De Michele, R. Schilling, and F. Sciortino, Phys. Rev. Lett. **98**, 265702 (2007).

[87] P. Pfeiderer, K. Milinkovic, and T. schilling, Europhys. Lett. **84**, 16003 (2008).

[88] S. Kruger, H.J. Mogel, M. Wahab, and P. Schiller, Langmuir **27(2)**, 646 (2011).

Chapter 2

Experimental

As discussed in the previous chapter, our aim was to investigate the self-assembly and dynamics of colloidal ellipsoids of aspect ratio, $\alpha = 2.1$ in quasi 2-dimensions (2D). This chapter covers the synthesis of spherical as well as ellipsoidal polysterene (PS) particles following the protocols reported by Ho *et al.* in 1993.[1]

2.1 Synthesis of PS Spheres

Uncrosslinked PS particles were synthesized via a free-radical polymerisation technique.[1] Presence of oxygen inhibits polymerisation and hence the reaction was carried out in nitrogen atmosphere. 167.5 ml of 25 mM sodium chloride (NaCl) was taken in a 3-necked round bottom flask which was placed in an oil bath and stirred at 350 rpm. The system was left to stabilize at 80°C for 15 minutes. Then 20 ml of distilled styrene (Sigma Aldrich) was added to the reaction pot. After equilibration, 38 mg of initiator (here potassium persulfate) dissolved in 7.5 ml of water, was added to the reaction pot. The solution slowly turned turbid signifying the onset of polymerisation. The reaction continued for 24 hours. The system was then cooled and filtered using glass wool to remove large aggregates. The particles were cleaned

by repeated centrifugation at 3000 rpm and redispersal in water (Milli Q). To estimate the particle size, the particles were allowed to crystallize using a depletion interaction and the lattice constant estimated from optical microscopy was found to be 1.4 μm.

2.2 Synthesis of PVA

Since uncrosslinked PS particles are thermoplastic, they could be deformed to a desired shape when heated beyond their glass transition temperature T_g (for PS $T_g = 100°$C). To stretch these PS spherical particles, we need a film forming material like PVA that acts as a matrix in which the spherical particles can be embedded. For the synthesis of PVA, we followed the protocol by Ho *et al.*[1] 15 g of polyvinyl acetate, PVAc, (Sigma Aldrich, Mol. wt. 5,00,000) was dissolved in 250 ml of methanol and water solution (1:4 v/v). The solution was stirred for 2-3 days which allowed most of the PVAc to dissolve. To this system, 2.25 g of sodium hydroxide (NaOH) was added and refluxed for 4 hours at 105° C. The solution was neutralized using concentrated hydrochloric acid (HCl) and $\sim$ 200 ml of isopropanol was added till a saturated white gel was obtained. We discarded the supernatant carefully and soaked the gel in water and washed it repeatedly for 24 hours at an interval of 2-3 hours. Then, 165 ml of isopropanol:methanol:water solution (6:1:4 v/v) was added to the gel and heated it gradually from 35°C to 80°C with continuous stirring at 200 rpm. The gel dissolved completely in this solution within 2-3 hours. The viscous solution of PVA was dialysed using a dialysis membrane in water environment and water was changed $\sim$ 10 times, after every 2-3 hours.

2.3 Film Formation and Ellipsoid Synthesis

We used a perspex tray of size 13 cm x 9 cm to make the films. 500 μl of PS spherical colloidal suspension (20-30% volume fraction) was dissolved in 50 ml of PVA. The above solution was poured slowly into the perspex tray and then placed inside the vacuum oven. The solution was allowed to stabilize at 28°C and 0.1 atm. After 2 days, the temperature was ramped to 45 °C in steps of 2.5 °C every 12 hours to avoid any bubble formation during the drying process. The film takes 4-5 days to get dry. For uniform stretching, the smooth film was cut into strips of dimension 4 cm x 6 cm. To achieve a better control on uniformity of stretched PS particles, square grids of dimension 0.5 cm x 0.5 cm were marked on the strips as shown in Figure 2.1. The film was clamped to a home made film-stretching apparatus as

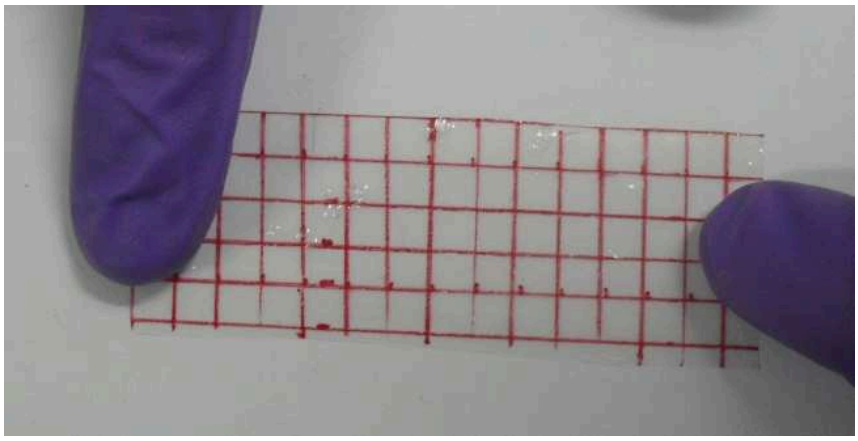

Figure 2.1: Unstretched PVA film with PS spherical particles embedded in it. The red lines marks the square grids of size 0.5 cm x 0.5 cm.

shown in Figure 2.2.

The film-stretching apparatus was dipped into an oil-bath maintained at 180°C. We manually stretched the film uniaxially to a draw ratio of 3 (Figure 2.3). The apparatus was taken out and allowed to cool down to room temperature. Only rectangular grids of same aspect ratio were taken for recovery of the ellipsoidal particles (Figure 2.3). The oil on the film was cleaned thoroughly using soap solution

Figure 2.2: Stretching apparatus built in our lab. The film is clamped in between two steel blocks as shown and stretching is done manually.

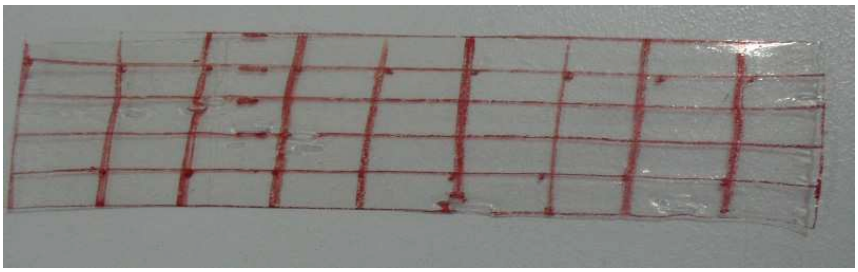

Figure 2.3: Stretched film. The square grids prior to stretching have changed to rectangles depending on the draw ratio.

(labolin) and rinsed with an excess of distilled water. To extract the ellipsoidal particles, the film was soaked in a solution of isopropanol:water (3:7 v/v) overnight and then refluxed at 80°C for 4-5 hours. The film completely dissolved and the resulting turbid suspension was centrifuged at ∼3000 rpm to allow the colloidal particles to settle to the bottom of the centrifuge tube. The supernatant was discarded and the particles were redispersed in isopropanol-water solution and again refluxed at 80°C for 5 hours to remove any traces of PVA. The suspension was cleaned repeatedly using milli Q water (TKA, 18.2MΩ). FESEM measurements were done to obtain the aspect ratio of our ellipsoids (Figure 2.4). From the analysis of over 100 ellipsoids we found that the major and minor axes are $l = 2.1$ μm and $w = 1.0$ μm with polydispersity of 11% and 8% respectively.

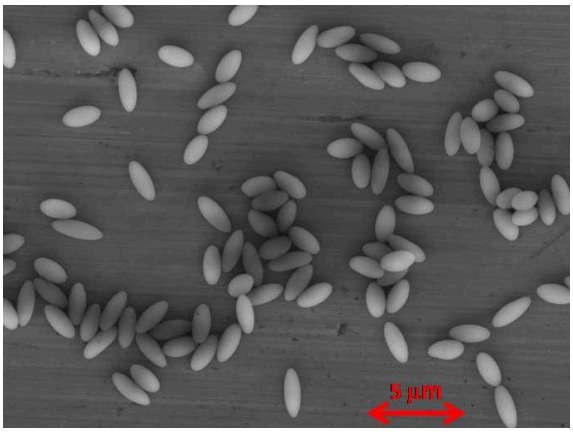

Figure 2.4: FESEM images of the ellipsoids. The scale bar is 5 μm.

We have used sodium carboxyl methyl cellulose (NaCMC, Fischer-Scientific, Mol. wt. 700000) as the depletant. Using Kramer's equation[2] the overlap concentration c^* of the depletant, from rheological measurements, was found to be $c^* = 0.11$ mg/ml. The highest depletant concentration c_p studied in our work was $c_p = 0.05$ mg/ml which is less than c^*. Using well established the scaling arguments,[2] we estimated the radius of gyration of the depletant to be 60 nm.

2.4 Experimental Cell and Imaging

The suspension of ellipsoids at suitable depletant concentration c_p was loaded in a wedge-shaped cell (Figure 2.5). The cells were left standing for sedimentation of

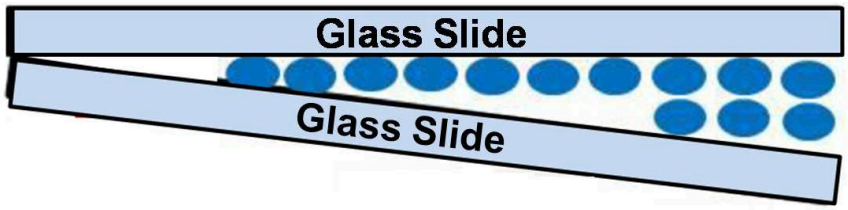

Figure 2.5: Schematic of the wedge cell with ellipsoids (blue color) loaded in it. The thin regions of the cell are quasi 2-dimensional (not to scale).

particles to the thin regions of the cell. Video microscopy was done using a 100X oil immersion objective (Leica, Plan-Apochromat, N.A. 1.4) at a frame rate of 5 fps for a typical duration of 20 minutes. The data for $\phi = 0.84$, for the purely repulsive case, was taken at frame rate of 1 fps for 2 hours. To ensure that the viewing region was quasi 2-dimensional (2D), we analysed the change in major, Δl, and minor, Δw, axes of each ellipsoid in successive frames. A thick cell can support out of plane fluctuations of an ellipsoid which can result in an effective change in its aspect ratio, α, in the imaging plane as shown in Figure 2.6a. We find that the distributions of Δl and Δw are Gaussian with standard deviation of 0.03 μ m and 0.06 μm respectively as shown in Figure 2.6b and c. The small standard deviations along with the small depth of field of the microscope objective ($\sim$ 200 nm) show that the cells were indeed quasi 2D. The experiment was done in a typical viewing region of size 65 μm x 47 μm at six ϕs ranging from $0.23 < \phi < 0.84$.

The images were pre-processed using Image-J which yielded the coordinates of centre-of-mass and the orientations of each ellipsoid as shown in the Figure 2.7. The data was analysed using standard as well as custom developed Matlab codes.[3,4] To obtain the spatial and orientational tracking resolution in our experiments, we

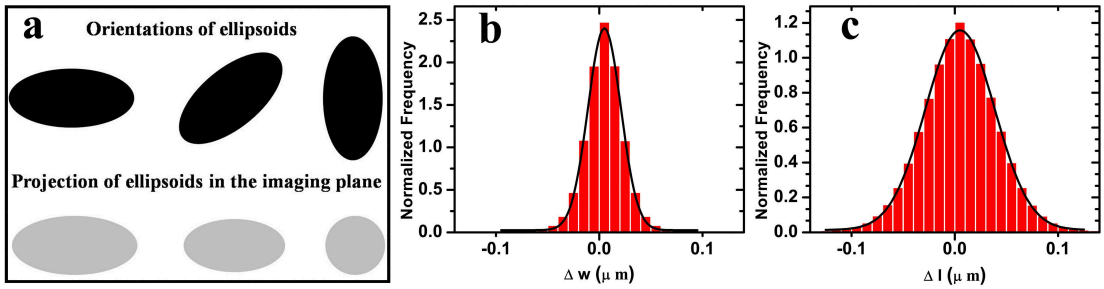

Figure 2.6: (a) Out-of-plane orientations of ellipsoid in a thick cell and their projections in the imaging plane. Distribution of the change in major axis Δl (b) minor axis Δw (c) of the ellipsoids between successive frames. The solid lines represents Gaussian fits to the distribution.

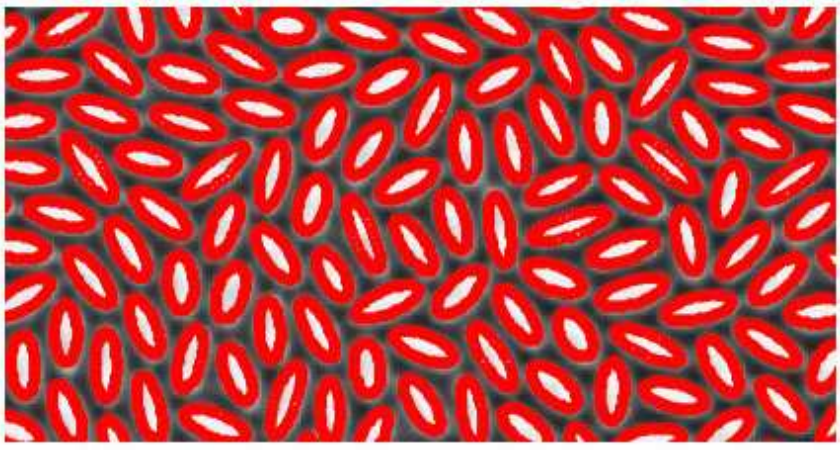

Figure 2.7: The image shows the tracking of the ellipsoid at $\phi = 0.79$. The red lines are the boundaries of the ellipsoids which have been drawn with the information obtained from Image-J

analysed the mean squared displacements $\langle \Delta r^2 \rangle$ and mean squared orientational displacements $\langle \Delta \theta^2 \rangle$ of the ellipsoids in very dilute regime ($\phi = 0.04$). The dynamics were observed to be diffusive for both translational and orientational degrees of freedom (Figure 2.8). The intercepts of $\langle \Delta r^2 \rangle$ and $\langle \Delta \theta^2 \rangle$ on the y-axes yielded the spatial and angular resolutions to be 60 nm and 1°, respectively.

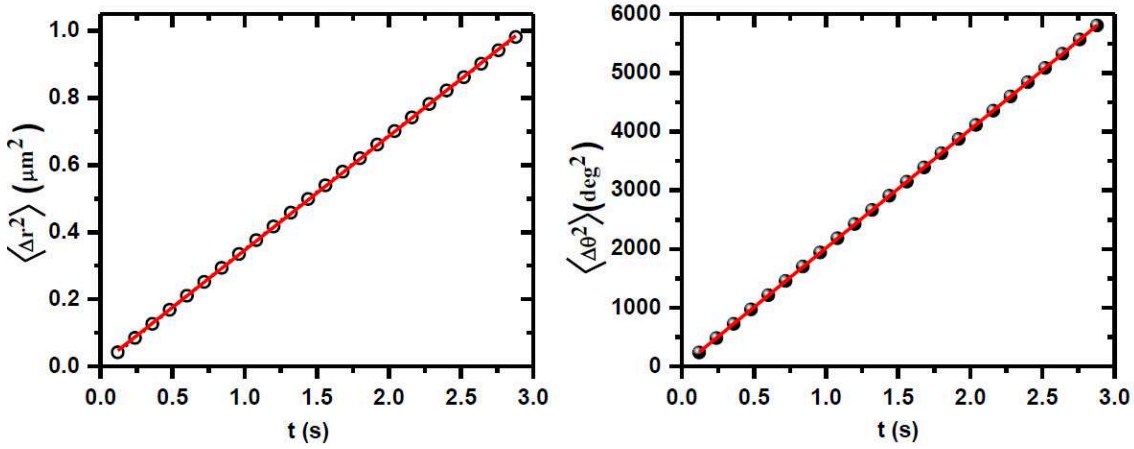

Figure 2.8: (a) $\langle \Delta r^2 \rangle$ *vs.* t at $\phi = 0.04$ and (b) $\langle \Delta \theta^2 \rangle$ *vs.* t at $\phi = 0.04$ for estimating the spatial and orientational resolution.

Bibliography

[1] C.C. Ho, A. Keller, J.A. Odell, and R.H. Ottewill, Colloid Polym. Sci **271**, 469 (1993).

[2] M Rubenstein, R. H. Colby, " Polymer physics", Oxford Univ. Press: New York (2003).

[3] J.C. Crocker and D.G. Grier, J. Colloid Interface Sci **179**, 298 (1996)

[4] See standard softwares (matlab codes) at http://people.umass.edu/kilfoil/downloads.html

Chapter 3

Depletion Attraction Induced Two-Step Glass Transition in Short Colloidal Ellipsoids

In chapter 1 we have discussed that the simplest possible deviation from a spherical shape gives rise to novel glass transition phenomena. In particular, ellipsoids with aspect ratio, $\alpha = 6$, showed a two-step freezing of dynamics.[1] The first corresponding to orientational freezing which is followed by translational freezing of dynamics at a higher area fraction, ϕ.[1] However, theory predicts a single glass transition for $\alpha \leq 2.5$,[2] due to strong coupling between translational and orientational degrees of freedom (DOF). Nevertheless, even in 2D, experiments are yet to observe a single glass transition for ellipsoids of $\alpha = 2.1$. Further, tuning the interaction potential in the spherical colloids from repulsive to attractive led to the observation of a novel glassy state viz. attractive glasses and reentrant glass dynamics.[3–11] The role of an anisotropic interaction potential on reentrant glass phenomena is yet to be explored by theory, simulations or experiments. This chapter presents a study on colloidal ellipsoid of $\alpha = 2.1$ in quasi 2-dimensions (2D) with an aim to explore reentrant

glass transition phenomena.

3.1 Ellipsoids with Purely Repulsive Interactions

Unlike observations on ellipsoids with $\alpha = 6$,[1] in our experiments, even after months, we did not observe the formation of pseudonematic domains even at the highest $\phi = 0.84$ studied (Figure 3.1). We have quantified the dynamics using translational and

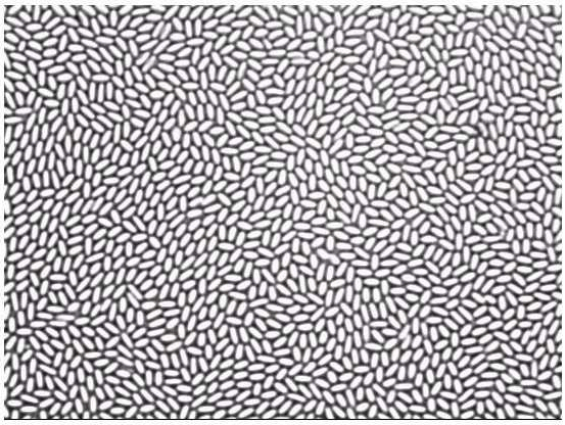

Figure 3.1: Representative image of colloidal ellipsoids at $\phi = 0.79$.

orientational correlation functions $F_s(\mathbf{q}, t)$ and $L_n(t)$, respectively. Glass transition area fraction(s) ϕ_g(s) were estimated using mode coupling theory (MCT) predictions.

The translational dynamics was quantified using the self-intermediate scattering function $F_s(\mathbf{q}, t)$ defined as:

$$F_s(\mathbf{q}, t) = \frac{1}{N}\langle \sum_{j=1}^{N} \exp[i\mathbf{q} \cdot (\mathbf{r}_j(t + t_0) - \mathbf{r}_j(t))] \rangle$$

Here, N is the total number of particles, $\mathbf{r}_j(t)$ is the position of the j^{th} ellipsoid at time t, t_0 is the lag time, $\mathbf{q}$ is the wave vector and the $\langle\rangle$ denotes the time averaging. The magnitude of q was chosen to be the first maximum in radial pair correlation function $g(r)$. The variation of $F_s(\mathbf{q}, t)$ as a function of ϕ is shown in Figure 3.2. At low ϕs, the system is fluid like as shown by the exponential decay of $F_s(\mathbf{q}, t)$. With increasing ϕ, particles become caged by their neighbours and this is

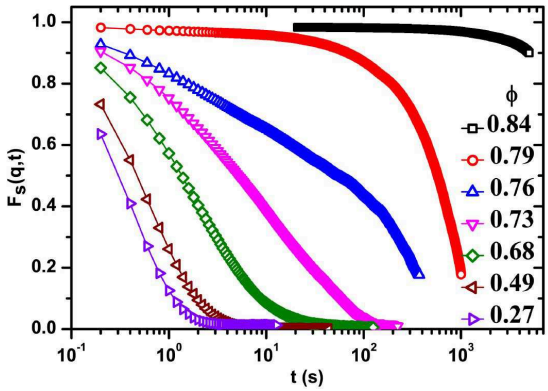

Figure 3.2: Self intermediate scattering function $F_s(q = 5.6\mu m^{-1}, t)$ at various area fractions ϕ.

reflected as a non-exponential decay in $F_s(q,t)$. For $\phi \geq 0.73$, the relaxation showed a two-step relaxation (Figure 3.2), a characteristic feature of supercooled liquids. While the first step corresponds to rattling of particles inside the cages formed by the neighbouring particles, the second corresponds to its subsequent escape from the cage. The first relaxation is termed as β-relaxation and the second one as α-relaxation.[12,13] While, for $\phi = 0.79$ $F_s(q,t)$ decayed almost completely over 700 s, for $\phi = 0.83$ it decayed only partially over an experimental time duration of 4000 s. This clearly indicates an ergodic to non-ergodic transition with $0.79 < {\phi_g}^T < 0.84$, where ${\phi_g}^T$ is the translational glass transition area fraction.

The orientational dynamics was quantified using the dynamic orientational correlation function $L_n(t)$ defined as,

$$L_n(t) = \frac{1}{N}\langle \sum_{j=1}^{N} P_n(\cos(\theta_j(t+t_0) - \theta_j(t)))\rangle$$

Here, N is the total number of particles, $\theta_j(t)$ is the orientation of the j^{th} ellipsoid at time t, t_0 is the lag time, $P_n(\cos(\theta))$ is the n^{th} order Legendre polynomial and $\langle\rangle$ denotes the time averaging. We have used the following three Legendre's polynomial,

$$P_3(x) = \tfrac{1}{2}(3x^2 - 3x)$$
$$P_4(x) = \tfrac{1}{8}(35x^4 - 30x^2 + 3)$$
$$P_5(x) = \tfrac{1}{8}(63x^5 - 70x^3 + 15x)$$

As observed for $F_s(q,t)$, $L_n(t)$ also showed exponential behaviour at low ϕs and onset of two-step relaxation and orientational caging beyond $\phi = 0.73$ (Figure 3.3). The decay in $L_n(t)$ was slower as compared to $F_s(q,t)$, signifying stronger caging effect on the rotational dynamics of particles in comparison to their translation motion. Similar to $F_s(q,t)$, while at $\phi = 0.79$, $L_5(t)$ decayed by $\approx 20\%$ over 700 s, for $\phi = 0.84$, it decayed by only 3% over 4000 s. This clearly indicated an ergodic to non-ergodic transition with orientational glass transition area fraction, with $0.79 < {\phi_g}^R < 0.84$. Hence, ϕ_g for both translational and orientational DOF lies in between $0.79 < {\phi_g}^{R,T} < 0.84$.

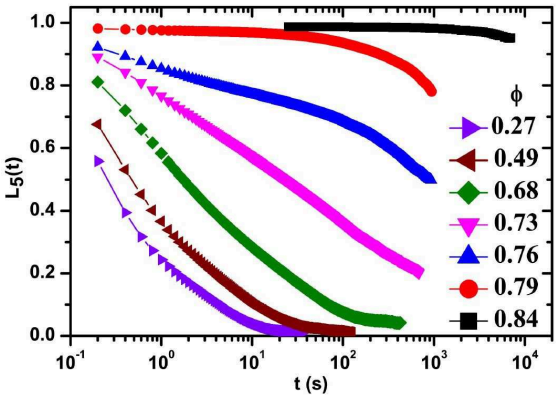

Figure 3.3: Dynamic orientational correlation function $L_5(t)$ at various area fractions ϕ.

We estimated the glass transitions for both the DOFs using MCT scaling analysis[1,12–14] mentioned in chapter 1. As per MCT, as ϕ_g is approached, relaxation time τ_α diverges as $\tau_\alpha(\phi) \propto (\phi_g - \phi)^{-\gamma}$ where $\gamma = \frac{1}{2a} + \frac{1}{2b}$. Here, a and b are exponents in the critical decay law and the von-Schweilder law, respectively.[1,15] In cases where $F_s(q,t)$ and $L_n(t)$ showed complete decay, τ_α was taken to be time where correlation decayed to $1/e$.[14,15] In cases where correlation functions showed only a partial decay but more than 70%, τ_α was calculated by fitting stretched exponential to long time decay of $F_s(q,t)$ and $L_n(t)$.[1] Further, it was verified that the two procedures yielded

the same τ_α. In our experiments, we obtained b from power-law fits to the cross-over regime from β to α-relaxation in $F_s(q,t)$ and $L_n(t)$. Owing to poor temporal resolution in the early β regime, we obtained a using the relation.[12]

$$\frac{\Gamma(1-a)^2}{\Gamma(1-2a)} = \frac{\Gamma(1+b)^2}{\Gamma(1+2b)}$$

Consistent with MCT predictions, we found that ${\tau_\alpha}^{-1/\gamma}$ was linear in ϕ (Figure 3.4) for all q's and n's studied. Strikingly, this scaling yielded the same $\phi_g = 0.80 \pm 0.01$ for both translational and orientational degrees of freedom (DoF) (Figure 3.4).

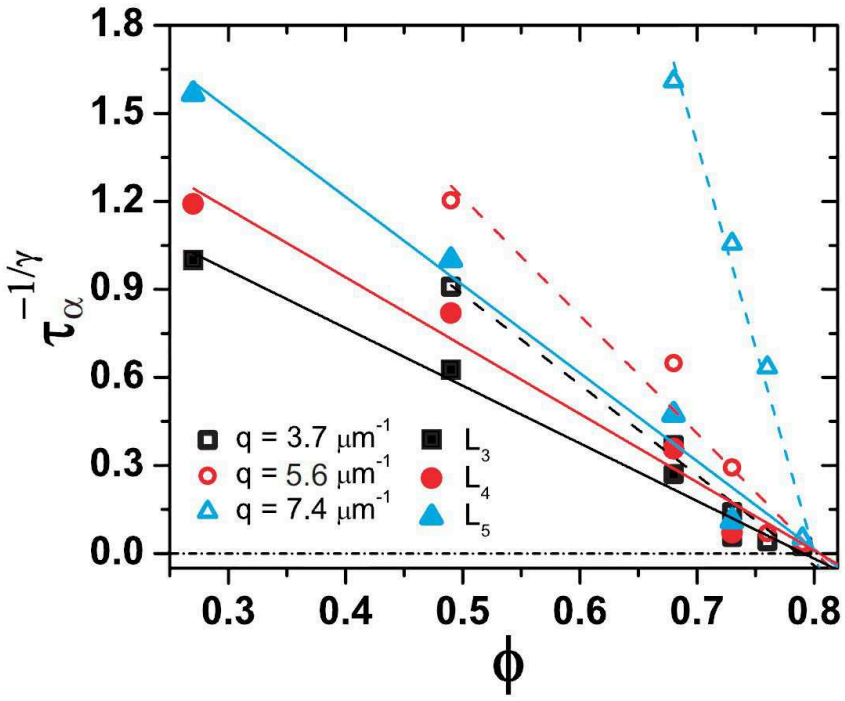

Figure 3.4: ${\tau_\alpha}^{-1/\gamma}$ *vs* ϕ. Here, $\gamma^T = 1.93$ and $\gamma^R = 2.04$. Dashed and solid lines are power law fits to the data, respectively.

To show that ϕ_g was indeed at 0.80 ± 0.01, we have quantified the size distribution and scaling of the most-mobile particle clusters. These clusters, believed to be pathways for structural relaxation in supercooled liquids and glasses,[16] show qualitative trends with ϕ across ϕ_g.[1,17] To quantify dynamical heterogeneities, we

first obtained the translational and rotational mean squared displacements (MSD) of the particles. The mean squared displacements ($\langle \Delta r^2 \rangle$) in 2D is defined as:

$$\langle \Delta r^2 \rangle = \frac{1}{N} \langle \sum_{j=1}^{N} [(x_j(t+t_0) - x_j(t))^2 + (y_j(t+t_0) - y_j(t))^2] \rangle$$

Here N is the total number of particles, $x_j(t)$ and $y_j(t)$ are the coordinates of j^{th} ellipsoid, t_0 is the lag time and Δr is the displacement of the particles over time t. The particle dynamics is diffusive at lower ϕs Figure 3.5. For $\phi \geq 0.73$, at short

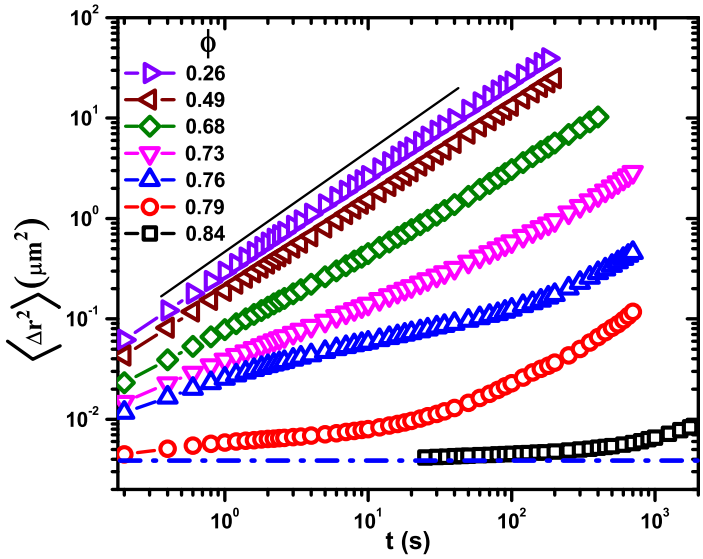

Figure 3.5: $\langle \Delta r^2 \rangle$ at various ϕ. The solid line has slope 1 and the dashed horizontal line represents the minimum tracking resolution in our experiments.

time, the dynamics is subdiffusive which signifies rattling of particles inside the cages (Figure 3.5). At characteristic relaxation time t^*, which is less than τ_α, $\langle \Delta r^2 \rangle$ showed an upturn which reflected the escape of particles from their respective cages (Figure 3.5). The long time dynamics after t^* approaches the diffusive limit.

The rotational dynamics, $\langle \Delta \theta^2 \rangle$, was quantified using :

$$\langle \Delta \theta^2 \rangle = \frac{1}{N} \langle \sum_{j=1}^{N} [(\theta_j(t+t_0) - \theta_j(t))^2] \rangle$$

Here, N is the total number of particles, $\theta_j(t)$ is the orientation of j^{th} ellipsoid, t_0 is the lag time and $\Delta\theta$ is the change in orientation of the particles over t. As shown in Figure 3.6, all the trends seen in $\langle \Delta r^2 \rangle$ (Figure 3.5) are also present in $\langle \Delta\theta^2 \rangle$.

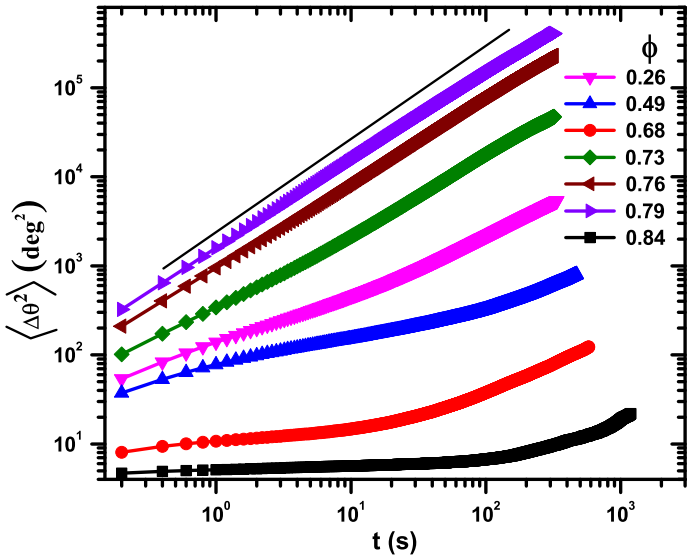

Figure 3.6: $\langle \Delta\theta^2 \rangle$ at various ϕ. The solid line represent the line of slope 1.

At t^* , the dynamics is highly non-Gaussian and this was quantified using the non-Gaussian parameter, $\alpha_2(t)$,[17] which is defined as,

$$\alpha_2^T(t) = \frac{\langle \Delta r(t)^4 \rangle}{2\langle \Delta r(t)^2 \rangle} - 1 \text{ and } \alpha_2^R(t) = \frac{\langle \Delta\theta(t)^4 \rangle}{3\langle \Delta\theta(t)^2 \rangle} - 1$$

where $\Delta r(t)$ and $\Delta\theta(t)$ are the particle displacements and change in orientations over time t, respectively. Since for any Gaussian process all the higher order moments can be expressed in terms of $\langle \Delta r^2(t) \rangle$, $\alpha_2^{T,R}(t) = 0$ for diffusive dynamics. However for supercooled liquids $\alpha_2^{T,R}(t)$ shows a maximum in the vicinity of t^* due to cage rearrangements (Figure 3.7)[17] (Figure 3.7). Both t^* and the peak amplitude $\alpha_2(t^*)$ increases as the glass transition is approached (Figure 3.7). In the vicinity of ϕ_g and beyond, the particle dynamics slow down as is evident from the plot of probability distribution of displacements of particles, $P(\Delta(r))$ over t^* (Figure 3.8). Thus, for ϕs

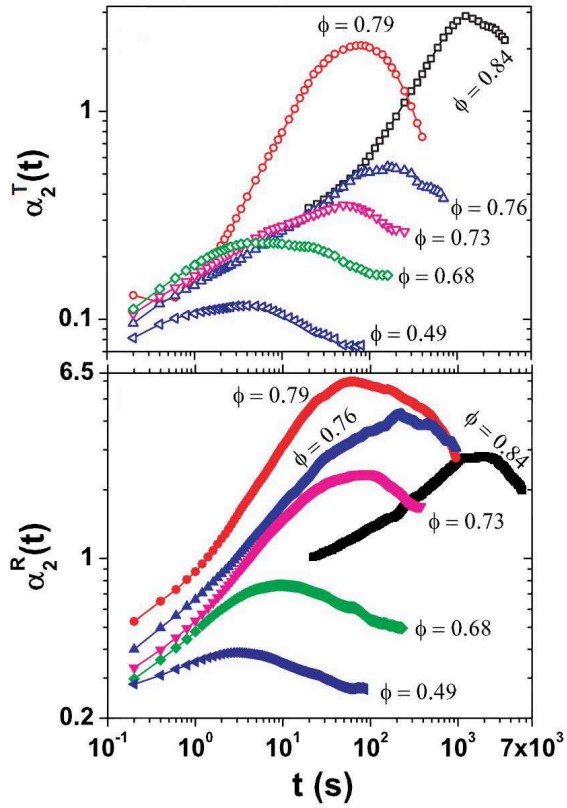

Figure 3.7: Non-Gaussian parameter $\alpha_2^T(t)$ (a) and $\alpha_2^R(t)$ (b) at various ϕ.

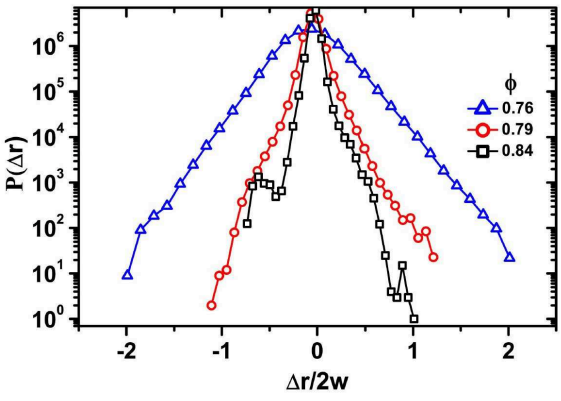

Figure 3.8: $P(\Delta r)$ *vs* Δr over t^* at three ϕ's in the vicinity of ϕ_g. Here t^* corresponds to the cage breaking time.

close to but less than ϕ_g, the absence of large cooperative cage rearrangements lead to a decrease in t^* [1,17] and was consistent with our observations of ${t^*}_{\phi=0.79} < {t^*}_{\phi=0.76}$. However, beyond ϕ_g, absence of large cooperative cage rearrangements should result in a decrease in both t^* and $\alpha_2(t^*)$. Unlike at low ϕs, t^* in the vicinity of ϕ_g and beyond is thought to represent the β-relaxation time.[17] Since $\alpha_2(t)$ is fairly sensitive to noise, the increase in t^* at $\phi = 0.84$, in our case, was probably due to particle tracking errors from negligible particle displacements that were comparable to the spatial resolution in our experiments.[18] It is important to note that the coupling between rotational and translational DOF can lead to non-Gaussian effects in the lab frame for ellipsoids even in the dilute limit.[19] We have verified that all trends reported here were preserved in the body frame of ellipsoids also, where this coupling is absent. The particle dynamics were heterogeneous over t^* as shown in the Figure 3.9. The top 10% most-mobile particles over t^* were found to be spatially clustered Figure 3.9. Two most-mobile particles belong to the same cluster if one

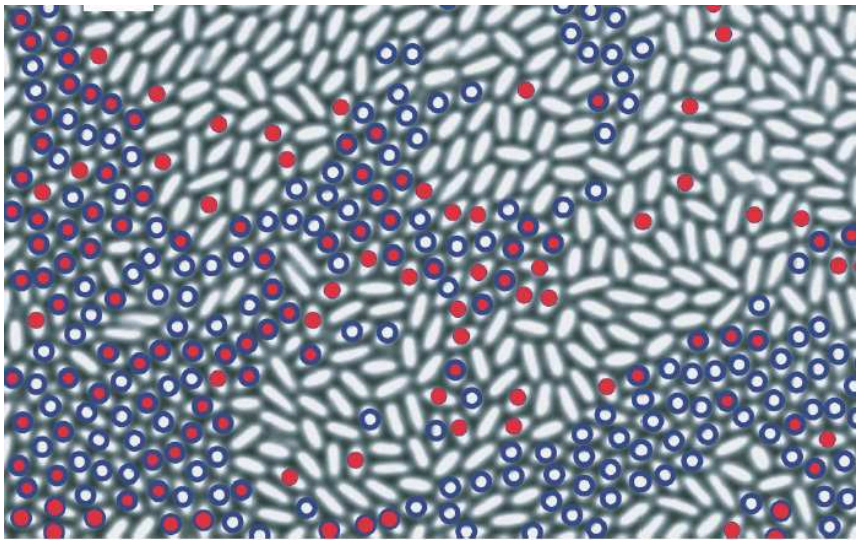

Figure 3.9: Top 10 % translationally most-mobile (open blue circles) and orientationally most-mobile (solid red circles) particles at $\phi = 0.79$.

ellipsoid when expanded 1.4 times, maintaining its orientation, encompasses the other's centre, subject to the condition that there is no immobile ellipsoid between

them. We found that a significant fraction of orientationally most-mobile particles were also translationally most-mobile and was consistent with the absence of pseudo-nematic domains (Figure 3.9).

To quantify these clusters at a given ϕ, we have used average cluster size $\langle N_c \rangle$[20] as:

$$\langle {N_c}^{T,R} \rangle = \frac{\sum_n n^2 P(n)}{\sum_n n P(n)}$$

where $P(n)$ is the cluster size distribution. Analogous to observations in glasses of spherical colloids,[17] $\langle {N_c}^{T,R} \rangle$ increases as ϕ_g is approached and shows a sudden decrease beyond ϕ_g for both translational and orientational DOF (Figure 3.10). These observations confirm that $0.79 < {\phi_g}^T, {\phi_g}^R < 0.84$ and is consistent with

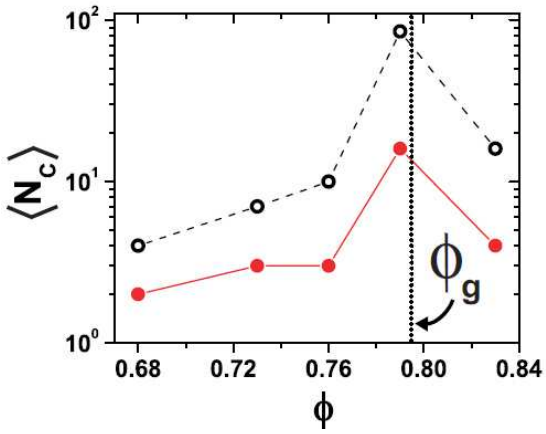

Figure 3.10: Average cluster size, $\langle N_c \rangle$ at different ϕ's. The vertical dashed line represents the glass transition area fraction ϕ_g

$\phi_g = 0.80 \pm 0.01$ estimated from MCT scaling analysis. Further, $\langle {N_c}^{T,R} \rangle$ diverges as a power law as ϕ_g is approached (Figure 3.11).

$$\langle {N_c}^{T,R} \rangle \propto (\phi_g - \phi)^{-\eta}$$

where η is scaling exponent. Though the physical origin of such a scaling is not clear, similar behaviour has also been observed for glasses of colloidal ellipsoids of $\alpha = 6$[1] and a binary Lennard-Jones glass forming liquid.[21] This further validates

our observation of a single ϕ_g for both translational and orientational DOF at $\phi = 0.80 \pm 0.01$.

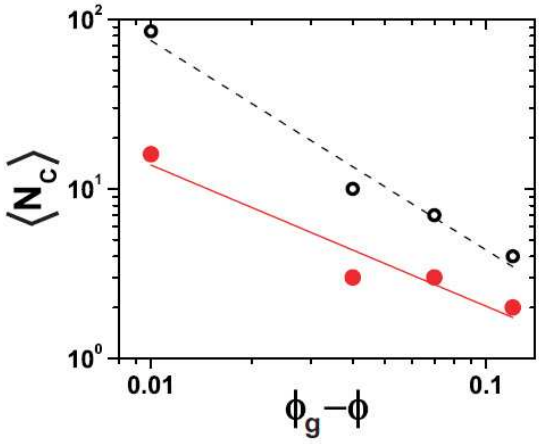

Figure 3.11: Divergence of average cluster size: $\langle N_c \rangle$ *vs* $(\phi_g - \phi)$.

Using the Vogel-Tammann-Fulcher (VTF) equation,[18,22,23] we have estimated the ideal glass transition area fraction ϕ_0 at which diffusive motion ceases,

$$\tau_\alpha(\phi) = \tau_\infty \exp \frac{A}{(1-\phi/\phi_0)}$$

Here, A and ϕ_0 are adjustable parameters. To determine ϕ_0, we have plotted the variation of residuals of linear fits as a function of ϕ_0 (inset to Figure 3.12). The minimum in the residuals for a given wave vector q corresponds to the best fit to the VTF equation. The average value of ϕ_0 obtained from two different values of q yields $\phi_0 = 0.89 \pm 0.02$ (Figure 3.12). As seen in previous studies,[18,22] the dynamic cross over area fraction ϕ_g determined from MCT scaling lies between the area fraction that corresponds to the onset of caging $\phi = 0.73$ and ϕ_0. Though there are no theoretical or computational predictions of ϕ_0 for ellipsoids of $\alpha = 2.1$, the value of ϕ_0 was in the vicinity of the predicted value ($\phi_0 \approx 0.88$) for bi-disperse ellipsoids, $\alpha \approx 2.2$, in 2D.[24]

In summary, colloidal ellipsoid of $\alpha = 2.1$ showed a single glass transition for both translational and orientational DOF at $\phi_g = 0.80 \pm 0.01$.

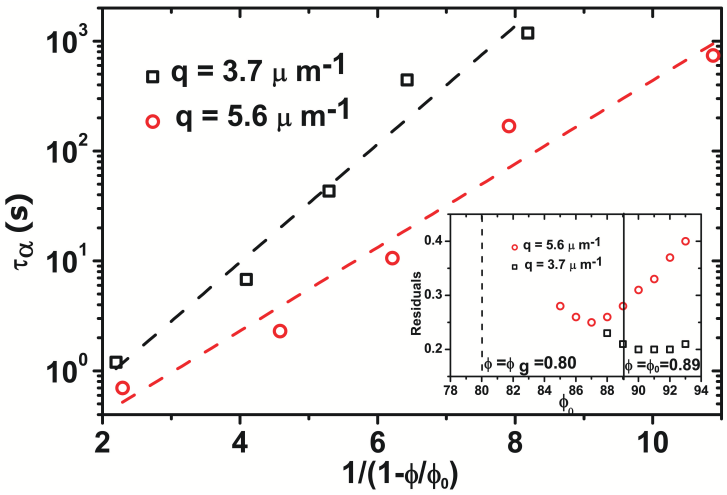

Figure 3.12: The scaling of relaxation time, τ_α with $(1-(\phi/\phi_0))$. The inset shows the residuals of the linear fits as a function of the fitting parameter ϕ_0. The dashed vertical line corresponds to ϕ_g for purely repulsive ellipsoids. The solid vertical line represents the average value of ϕ_0.

3.2 Hard Ellipsoids with Depletion Induced Attractive Interactions

While depletion induced attractions for spherical particles are isotropic,[25] it leads to an anisotriopic interaction for ellipsoidal particles.[26] Figure 3.13 clearly shows that ellipsoids prefer lateral alignment as compared to tip-to-tip alignment in presence of depletion induced attraction.

Here, our focus was on exploring the change in dynamics of colloidal ellipsoids as a function of particle pair potential, U. In 2D, the relationship between depletion concentration, c_p , and attraction strength U is not well-understood.[27] Therefore, for all c_ps investigated here, we directly measured the change in depth of the scaled depletion potential $\Delta u = -\frac{\Delta U}{k_B T}$, averaged over all orientations, with respect to $c_p = 0$, from dimer life time measurements.[28] Here, k_B is the Boltzmann constant and T is the temperature. To evaluate the change in the depth of attractive potential, Δu, we measured the monomer diffusion constant, D, and the dimer lifetime, τ,

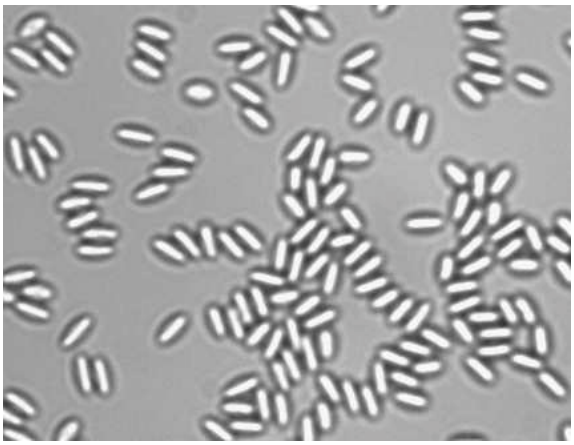

Figure 3.13: Image shows lateral alignment being promoted with turning on short-range depletion attraction

averaged over all orientations, at $\phi \approx 0.25$ for the various depletion concentrations, c_p, studied. The distributions of τ were observed to be exponential (Figure 3.14 b and c) and the decay constant yielded τ_0. However, for $c_p = 10$ μgml^{-1}, as the values of τ are small (Figure 3.14 a), τ_0 was taken to be the peak of the distribution. Following Savage *et. al.*,[28] we evaluated Δu using the τ_0 calculated above.

$$\tau_0 \propto D^{-1} exp(U/k_B T)$$
$$\frac{-\Delta(U_1 - U_2)}{k_B T} = \Delta u = ln(\frac{\tau_0^2 D_2}{\tau_0^1 D_1})$$

where 1 and 2 denote the two systems at different interaction strengths and all the other symbols have the usual meaning as introduced before. $\tau_0 D$ with c_p showed an exponential dependence (Figure 3.14 d), although the origin of this is unclear. Since, we could not collect data at $\phi \approx 0.25$ for $c_p = 30$ μgml^{-1}, the value of $\tau_0 D$ was obtained from fits to the data shown in the Figure 3.14 d.

Now, we will briefly show the dynamics, $\langle \Delta r^2 \rangle$ and $\langle \Delta \theta^2 \rangle$, of these ellipsoids at different Δus and a comparative study for reentrant glass dynamics will be presented in the next section. With the onset of depletion interactions, while the free volume enhances the dynamics till intermediate attractive strengths, the stronger bonding between particles slows the dynamics at higher attraction strengths as is clear from

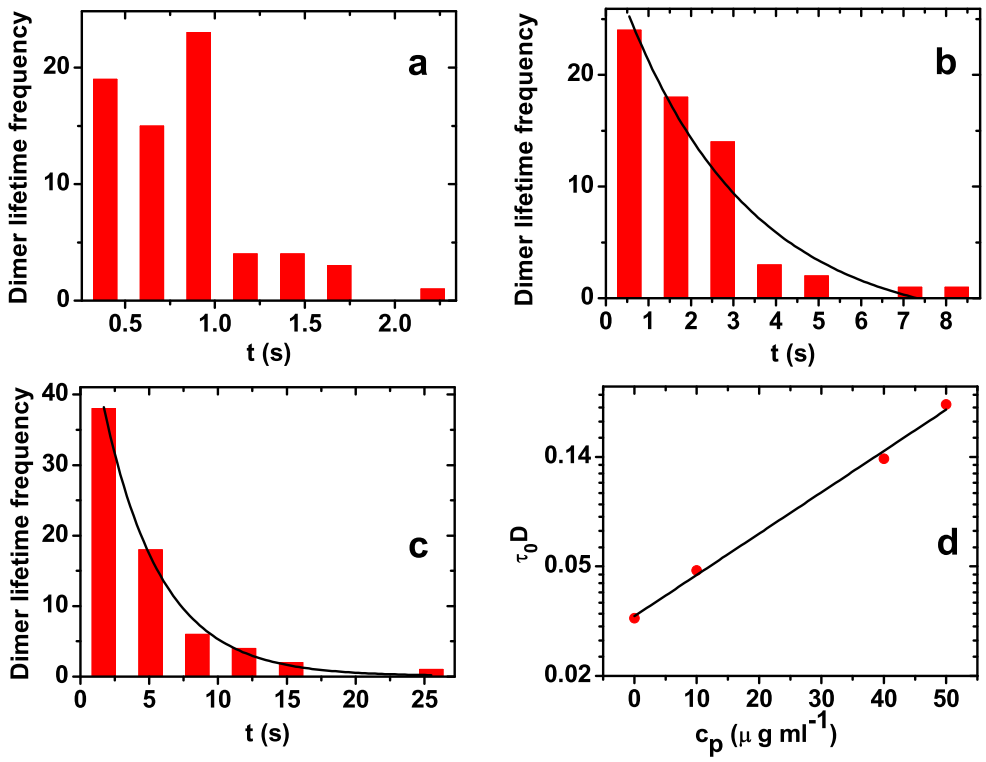

Figure 3.14: Distribution of dimer lifetimes for (a) $c_p = 10$ μgml^{-1} (b) $c_p = 40$ μgml^{-1} (c) $c_p = 50$ μgml^{-1}. The solid line in (b) and (c) shows exponential fits to the data. (d) Log-Linear plot of $\tau_0 D$ *vs* c_p. The solid line is linear fit to the data from which $\tau_0 D$ at $c_p = 30$ μgml^{-1} was obtained.

the plots of $\langle \Delta r^2 \rangle$ (Figure 3.15) and $\langle \Delta \theta^2 \rangle$ (Figure 3.16) at different Δu.

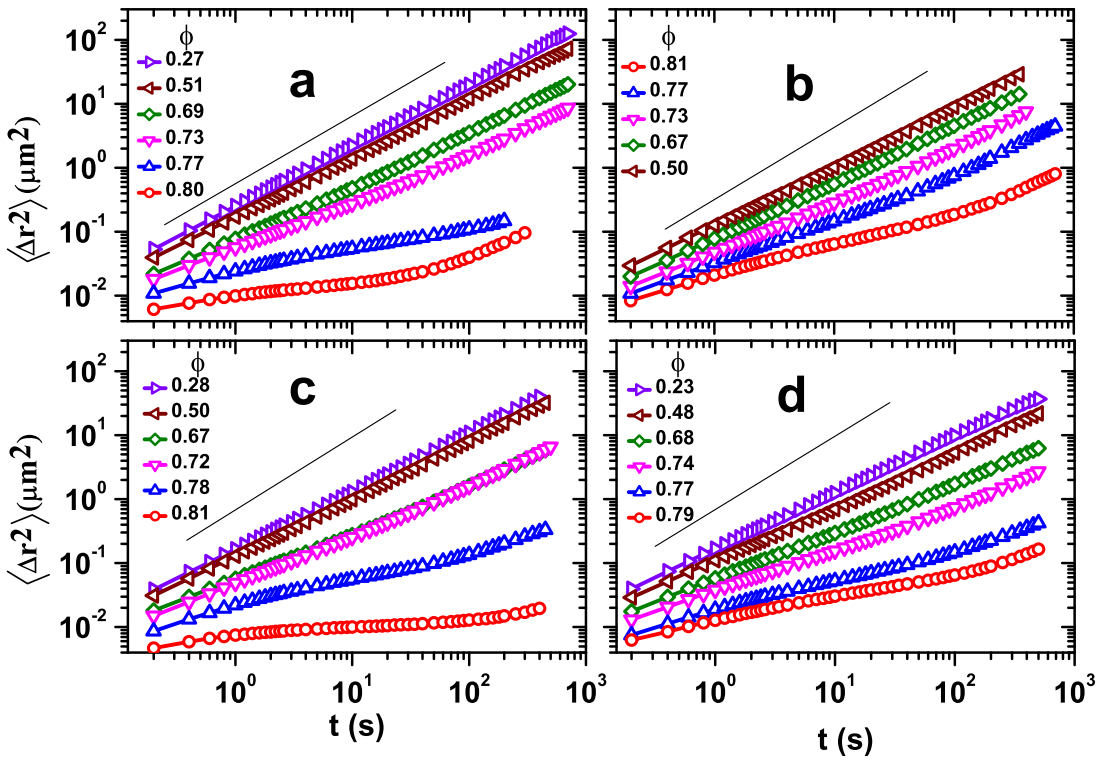

Figure 3.15: $\langle \Delta r^2 \rangle$ at different ϕ's and for $\Delta u = 0.44$ (a) $\Delta u = 1.16$ (b) $\Delta u = 1.47$ (c) $\Delta u = 1.95$ (d) The $\langle \Delta r^2 \rangle$ at $\phi = 0.67$ and $\phi = 0.72$ in (c) were observed to be same. The faster dynamics at $\phi = 0.72$ is attributed to thicker cell area in the viewing region.The solid lines in all sub-plots represent line of slope 1.

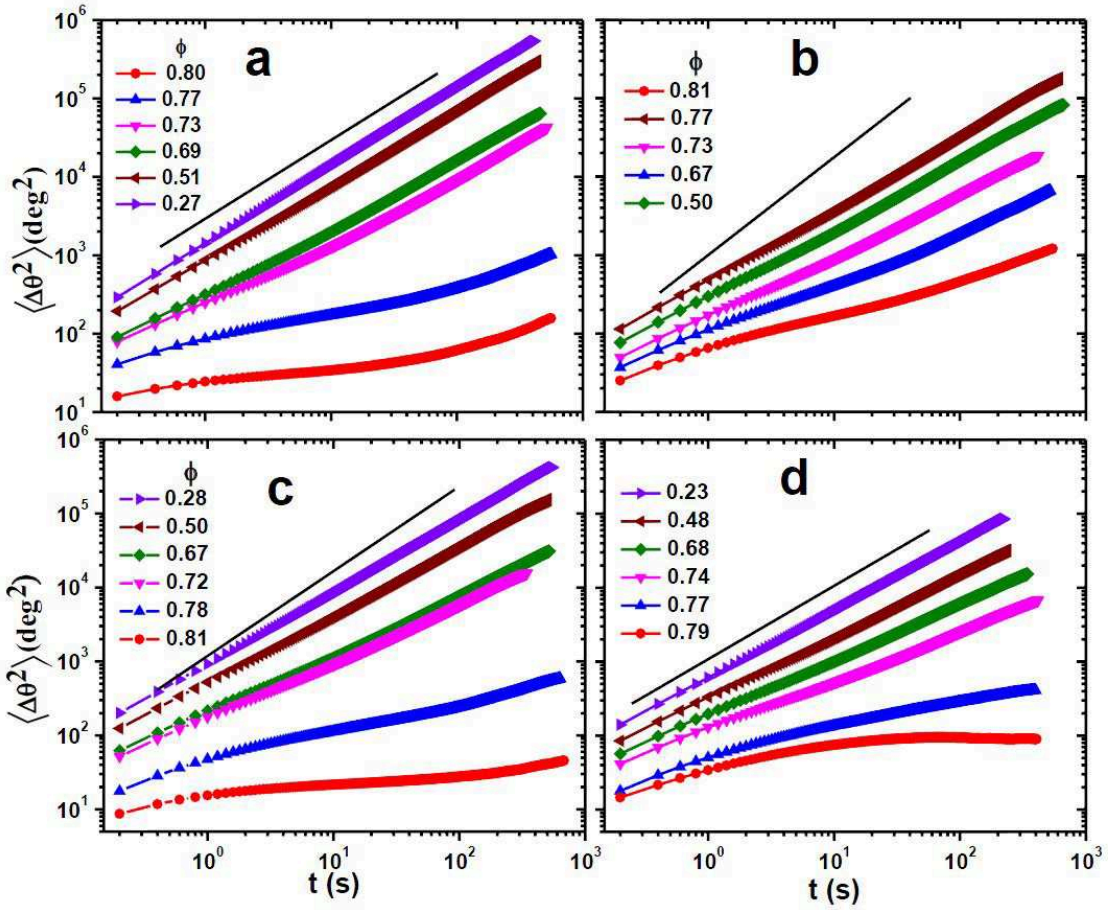

Figure 3.16: $\langle \Delta\theta^2 \rangle$ at different ϕ's and for $\Delta u = 0.44$ (a) $\Delta u = 1.16$ (b) $\Delta u = 1.47$ (c) $\Delta u = 1.95$ (d) The $\langle \Delta\theta^2 \rangle$ at $\phi = 0.67$ and $\phi = 0.72$ in (c) were observed to be same. The faster dynamics at $\phi = 0.72$ is attributed to thicker cell area in the viewing region. The solid lines in all sub-plots represent line of slope 1.

3.3 Reentrant Glass Dynamics in Hard Ellipsoids

In this section, we will discuss the change in translational and orientational dynamics of the colloidal ellipsoids as a function of particle interaction potential Δu at a $\phi \sim$ RG $\phi_g = 0.80$. We begin with the correlation functions $F_s(q,t)$ and $L_n(t)$. Figure 3.17a and b, shows $F_s(q = 5.6\mu\text{m}^{-1}, t)$ and $L_3(t)$ for $\phi \approx 0.79 \approx \phi_g$ for different Δus respectively. For $\Delta u = 0$ and $\Delta u = 1.47$, both $F_s(q,t)$ and $L_3(t)$ showed a two-step decay (inset to Figure 3.17 a and b). The larger plateau value at long times for

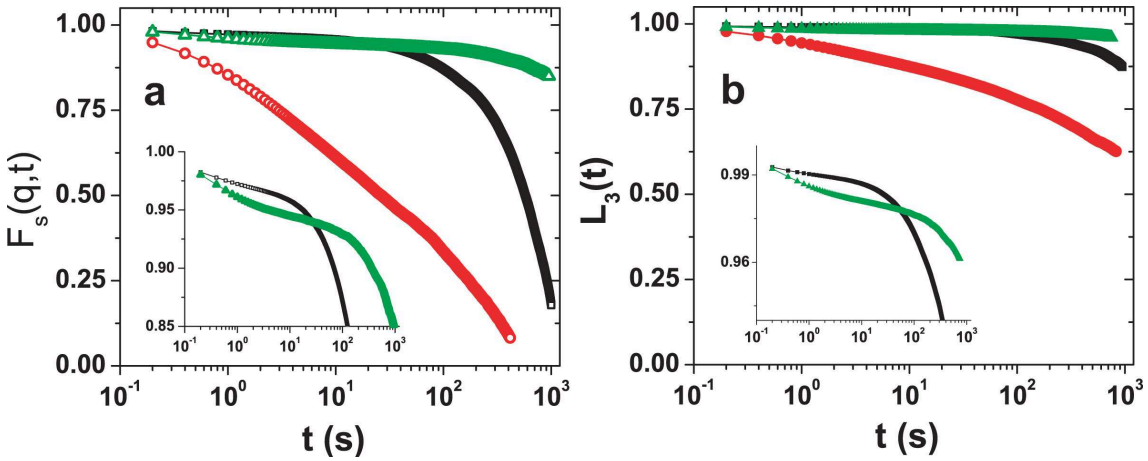

Figure 3.17: $F_s(q = 5.6\mu m^{-1}, t)$ and (b) $L_3(t)$ for $\Delta u = 0$ at $\phi = 0.79$ (black squares), $\Delta u = 1.16$ at $\phi = 0.81$ (red circles), $\Delta u = 1.47$ at $\phi = 0.81$ (green triangles). Inset to (a) and (b) - with expanded y-axis show two-step relaxation. Solid and open symbols correspond to orientational and translational scaling of τ_α, respectively.

$\Delta u = 1.47$ (Figure 3.17) implied a relatively stronger freezing-in of long-wavelength collective density fluctuations.[3,4] However, for an intermediate value $\Delta u = 1.16$, while $F_s(q,t)$ decayed completely (Figure 3.17a), only a partial decay was observed in $L_n(t)$ (Figure 3.17b). This indicates that the dynamics in translational and orientational DOF might be different. To ascertain if ϕ_g at intermediate attraction strength had indeed shifted to a $\phi >$ RG ϕ_g, we have performed the aforementioned MCT scaling for all Δus studied. In line with theoretical predictions,[8,9] ${\tau_\alpha}^{-1/\gamma}$ was

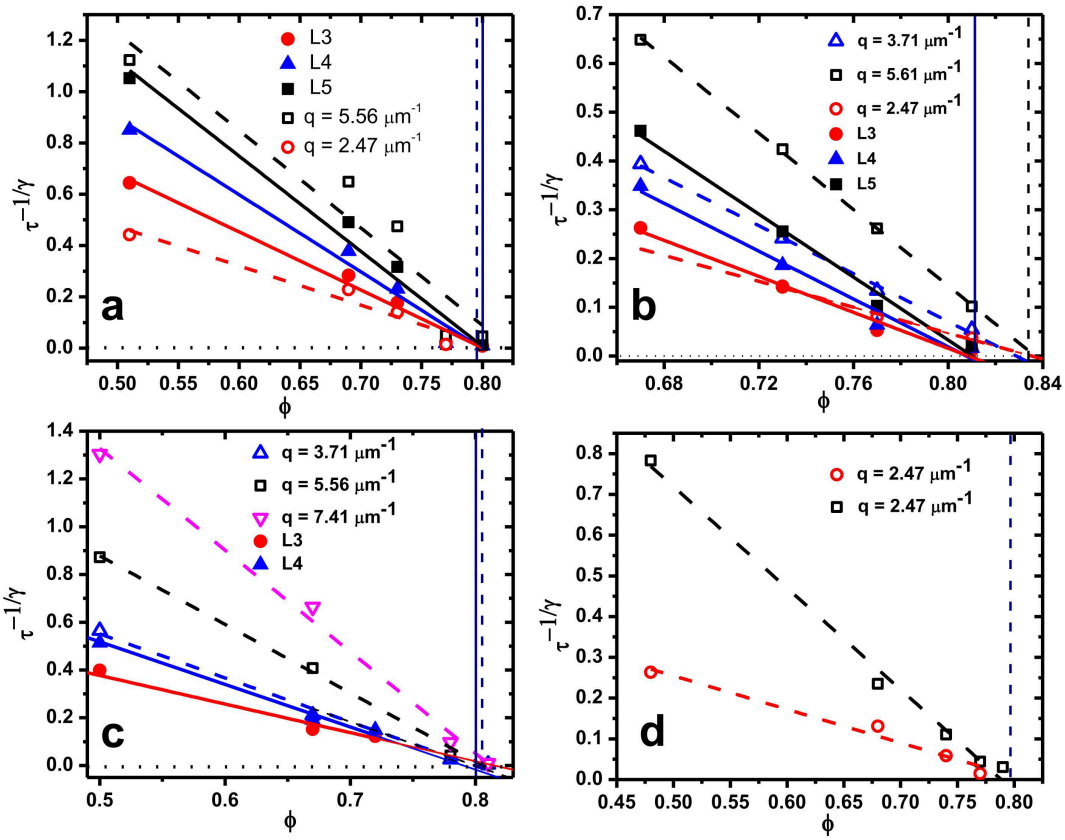

Figure 3.18: MCT scaling of τ_α for $\Delta u = 0.44$ (a), $\Delta u = 1.16$ (b), $\Delta u = 1.47$ (c) and $\Delta u = 1.95$ (d). Solid and open symbols correspond to orientational and translational scaling of τ_α, respectively. The lines are linear fits to the data. The solid and dashed vertical lines in (c) and (d) denote ${\phi_g}^R$ and ${\phi_g}^T$ respectively.

linear in ϕ for attractive glasses too and allowed us to extract ${\phi_g}^R$ and ${\phi_g}^T$ (Figure 3.18). Strikingly, for $\Delta u = 1.16$, we observed a two-step glass transition with ${\phi_g}^R = 0.81 \pm 0.01$ and ${\phi_g}^T = 0.84 \pm 0.01$ (Figure 3.18b). For $\Delta u = 1.47$, ${\phi_g}^T$ reverted to a lower ϕ with ${\phi_g}^T = 0.81 \pm 0.01$ and ${\phi_g}^R = 0.80 \pm 0.02$ (Figure 3.18c). Due to strong hindrance in rotation of the particles for $\Delta u = 1.95$, $L_n(t)$'s did not decay over the experimental time duration. Hence, we could not estimate the ϕ_g^R for $\Delta u = 1.95$.

To further validate the above observations, we explored the complete phase diagram in the $(\phi, \Delta u)$ plane with $\alpha_2^{T,R}(t = t^*)$, $F_s(q, t_\infty)$ and $L_3(t_\infty)$ as the quantifiers of particle dynamics. Here, t_∞ denotes the experimental time duration. Figure 3.19 shows the translational and orientational phase diagrams, along with MCT predicted glass transitions. Since, sedimentation to the 2D regions of the cell was extremely slow for ellipsoids with attractive interactions, we were unable to collect data beyond $\phi \approx 0.81$. Overall, $\alpha_2^T(t^*) < \alpha_2^R(t^*)$ indicating that the orientational relaxations were relatively more hindered as compared to the translational ones (Figure 3.19). While at low ϕ and at small Δus, an ergodic phase was observed, for large Δus, we found percolating networks of ellipsoids which we identified as a gel phase (Figure 3.20).[3,4]

Most remarkably, at a fixed $\phi \geq$ RG ϕ_g and with increasing Δu, while we observed a minimum in $\alpha_2^T(t^*)$ (Figure 3.19 a) at intermediate attraction strengths, we did not see this for $\alpha_2^R(t^*)$ (Figure 3.19 b). This clearly implies a melting of the glass only in the translational DoF and is consistent with our observations that in contrast to $F_s(q, t_\infty)$ (Figure 3.17 a), $L_n(t_\infty)$ (Figure 3.17 b) shows only a partial decay. Lending further credit to these observations, while the MCT predicted ${\phi_g}^T$ shows systematic reentrant behavior (Figure 3.19 a), within experimental certainty, ${\phi_g}^R$ (Figure 3.19 b) does not. Thus, inspite of having a single glass transition in the purely repulsive limit, reentrant behavior in translational and orientational DoF

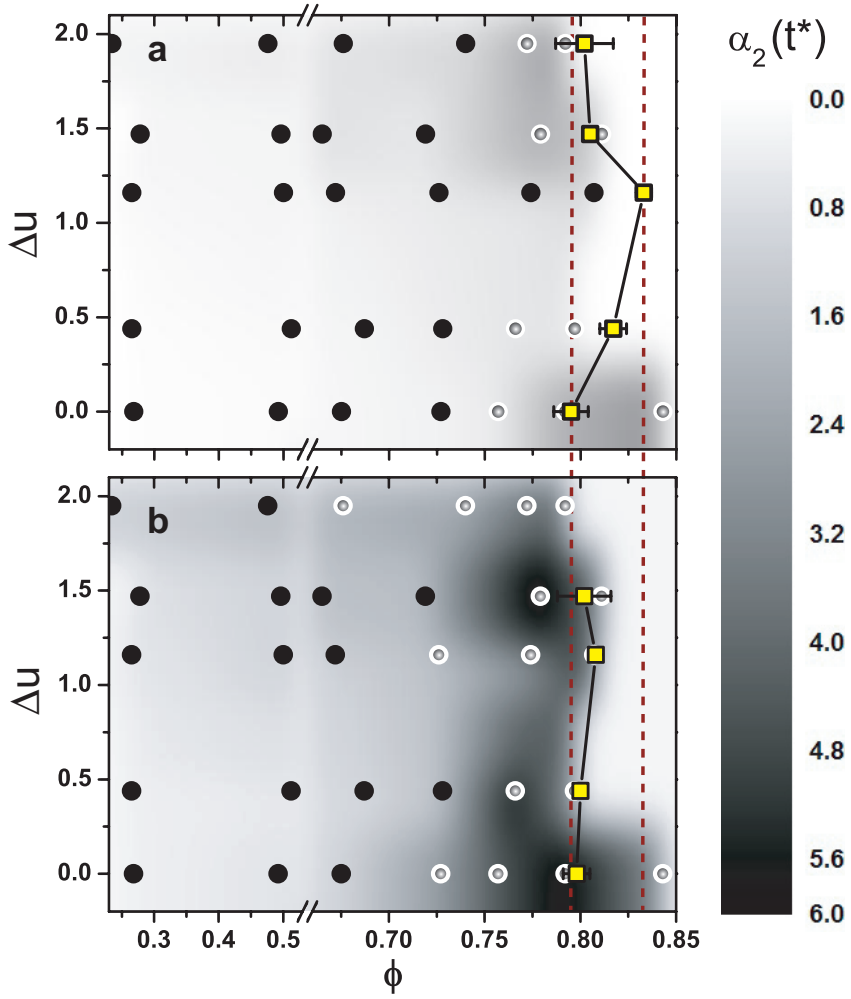

Figure 3.19: Phase diagram in $(\Delta u, \phi)$ plane. The circles represent the Δu and ϕ at which experiments were performed. (a) Translational DoF. (b) Orientational DoF. The black circles denote $F_s(q, t_\infty)$ and $L_3(t_\infty)$ that decayed completely. The white circles denote $F_s(q, t_\infty)$ and $L_3(t_\infty)$ that decayed partially. The color bar indicates the value of $\alpha_2(t = t^*)$. $\alpha_2^{T,R}(t^*)$ for ϕ's in between experimental data points were obtained from linear interpolation. Note the break in ϕ-axis at $\phi \approx 0.53$. ${\phi_g}^T$ and ${\phi_g}^R$, obtained from MCT scaling analysis, are shown by squares in (a) and (b) respectively.

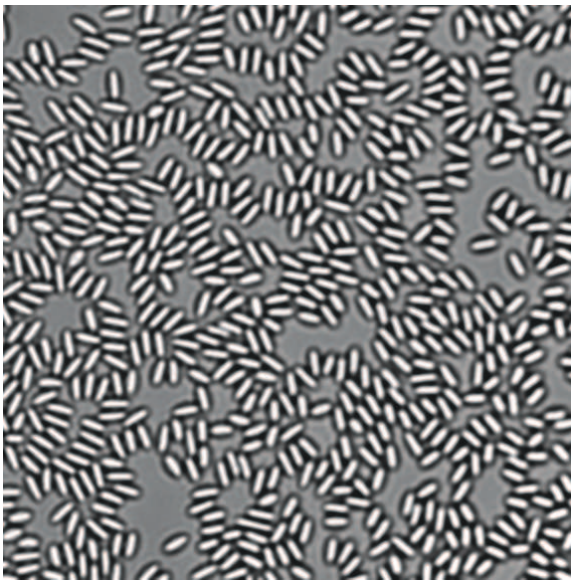

Figure 3.20: Representative image of the gel phase at $\phi = 0.47$ and $\Delta u = 1.95$.

were clearly different.

3.4 Rationalising Our Observations

Why do we see a two-step glass transition for intermediate Δu*?* To address this question, we quantified the structure and dynamics in the body frame of ellipsoids for $\phi \approx$ RG ϕ_g with increasing Δu. The structure was isotropic for $\Delta u = 0$ (Figure 3.21 a). While, for $\Delta u = 1.16$, depletion enhanced lateral alignment of ellipsoids resulting in quasi-long range ordering (Figure 3.21 b); for $\Delta u = 1.47$, the longer bond lifetime precluded the ellipsoids from sampling various configurations and led to smaller domain sizes (Figure 3.21 c). These variations in structure with increasing attraction strengths have been quantified using the pair correlation function, $g(r)$ (Figure 3.22). The absence of peak at $\frac{r}{2w} = 1.7$, confirms that perpendicular alignment of the ellipsoids are absent for $\Delta u = 1.16$ (Figure 3.22). Further, we have also quantified the static orientational correlation function, $g_2(r)$[29] defined as:

$$g_2(r) = \langle cos(2[\theta(0) - \theta(r)]) \rangle$$

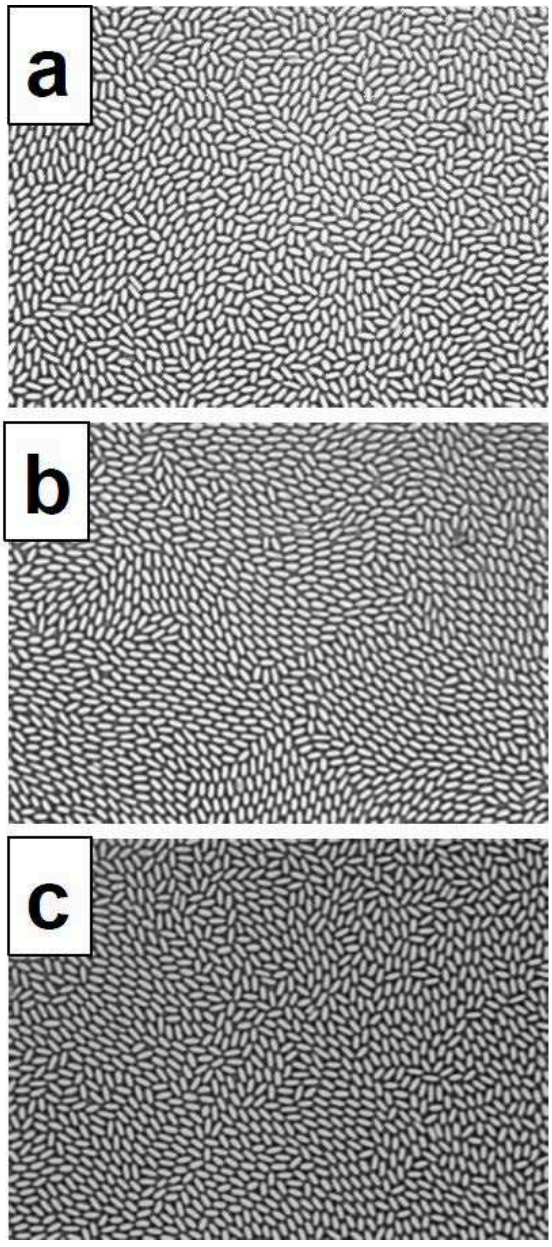

Figure 3.21: Representative images showing structure at (a) $\Delta u = 0$ at $\phi = 0.79$, (b) $\Delta u = 1.16$ at $\phi = 0.81$ and (c) $\Delta u = 1.47$ at $\phi = 0.81$.

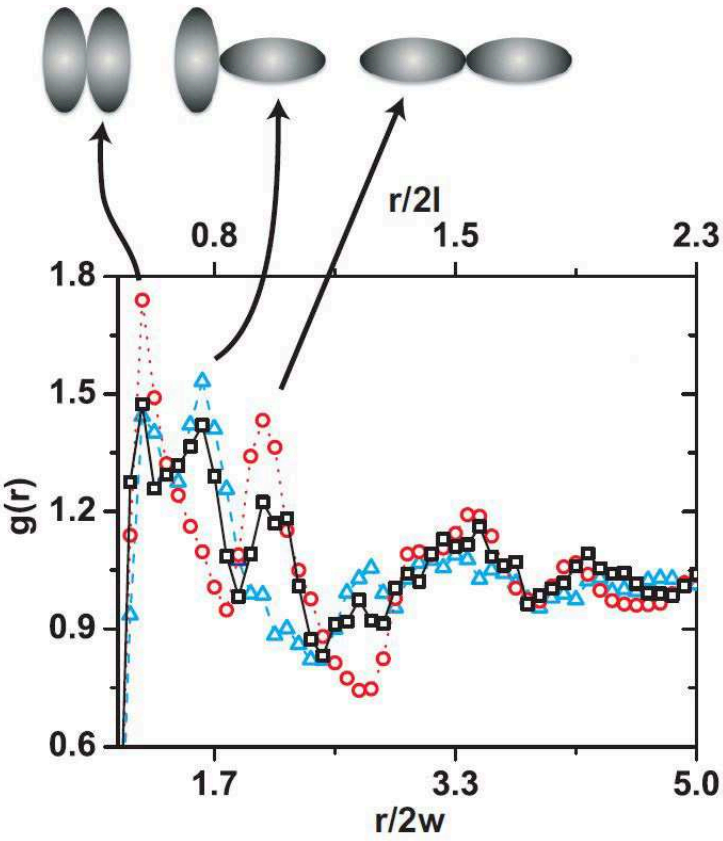

Figure 3.22: Pair correlation function $g(r)$ for $\Delta u = 0$ at $\phi = 0.79$ by black squares, $\Delta u = 1.16$ at $\phi = 0.81$ by red circles, and $\Delta u = 1.47$ at $\phi = 0.81$ by cyan triangles.

where θ is the orientation of the ellipsoid and r is centre-to-centre distance between two ellipsoids and $\langle\rangle$ denotes the ensemble averaged over all pairs of ellipsoids located at distance r. The higher value of $g_2(r)$ at $\frac{r}{2w} = 1.7$ was a clear indication of quasi-long range ordering (QLRO) at intermediate $\Delta u = 1.16$ (Figure 3.23).

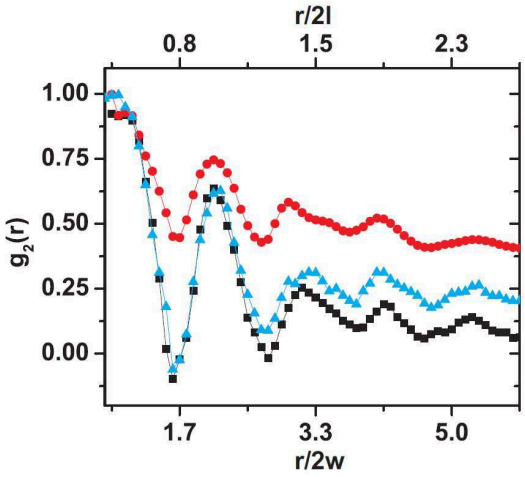

Figure 3.23: Static orientational correlation function $g_2(r)$ for $\Delta u = 0$ at $\phi = 0.79$ by black squares, $\Delta u = 1.16$ at $\phi = 0.81$ by red circles, and $\Delta u = 1.47$ at $\phi = 0.81$ by cyan triangles.

Apart from the analysis of $g(r)$ and $g_2(r)$, our arguments of QLRO at intermediate Δu was also supported by the analysis of dynamics in the bodyframe of ellipsoids. We have followed Han *et. al.*[19] to construct the trajectories in the bodyframe. Briefly, displacements of particles between two successive frames in the labframe were resolved along the major and minor axes of the ellipsoids. These displacements along the major and minor axes were summed to obtain the complete trajectory for a given ellipsoid. From these constructed trajectories, we have evaluated the MSD along major ($\langle \Delta r^2 \rangle_l$) and minor ($\langle \Delta r^2 \rangle_w$) axes of ellipsoids. As shown in Figure 3.24, the anisotropy in diffusion ($\frac{\langle \Delta r^2 \rangle_l}{\langle \Delta r^2 \rangle_w}$) is enhanced at $\Delta u = 1.16$ due to the relatively unhindered motion of the ellipsoids along their major axes within the domains. The time at which $\frac{\langle \Delta r^2 \rangle_l}{\langle \Delta r^2 \rangle_w}$ peaks in Figure 3.24 is the cage realaxation time t^*, as discussed in earlier sections. Since the diffusion was anisotropic, especially at

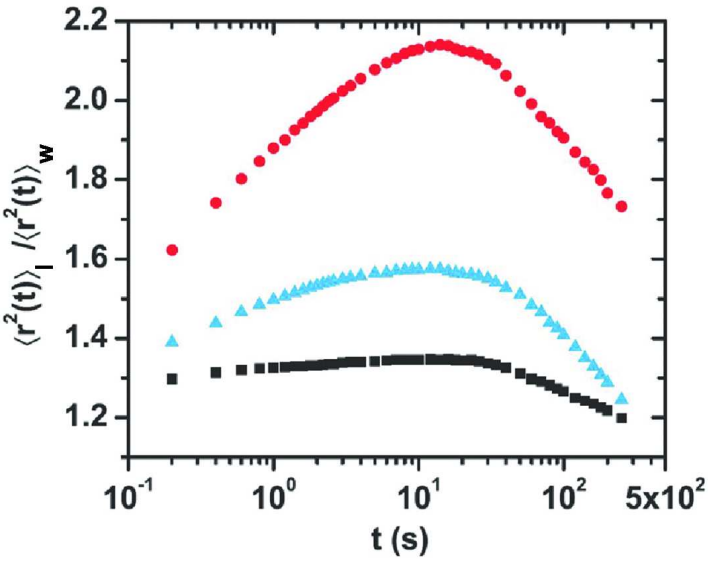

Figure 3.24: Ratio of mean-squared displacements along major and minor axis of ellipsoids for $\Delta u = 0$ at $\phi = 0.79$ by black squares, $\Delta u = 1.16$ at $\phi = 0.81$ by red circles, and $\Delta u = 1.47$ at $\phi = 0.81$ by cyan triangles.

intermediate attraction strengths, the cage relaxations were predominantly due to relaxation along the major axes of ellipsoids. Thus, while inter-particle attractions free up volume and shift ${\phi_g}^T$ to a higher $\phi = 0.84 \pm 0.01$, quasi-long range ordering hinders rotational relaxation and results only in a marginal shift in ${\phi_g}^R = 0.81 \pm 0.01$. Further, we find that the orientationally most-mobile particles are predominantly at inter-domain boundaries and the transnationally most-mobile particles are in the ordered regions as observed for colloidal ellipsoids of $\alpha = 6$ (Figure 3.25).[1]

In conclusion, our experiments highlight for the first time, the crucial role of particle shape and interaction anisotropy in reentrant glass phenomena. We have shown that 2D suspensions of colloidal ellipsoids ($\alpha = 2.1$) with purely repulsive interactions show a single glass transition. This is in qualitative agreement with MMCT predictions in 3D.[2] Owing to the lack of pseudonematic ordering, we find that an appreciable fraction of orientationally most-mobile particles are also transnationally most-mobile. Confirming theoretical predictions,[8,9] we found that MCT scaling

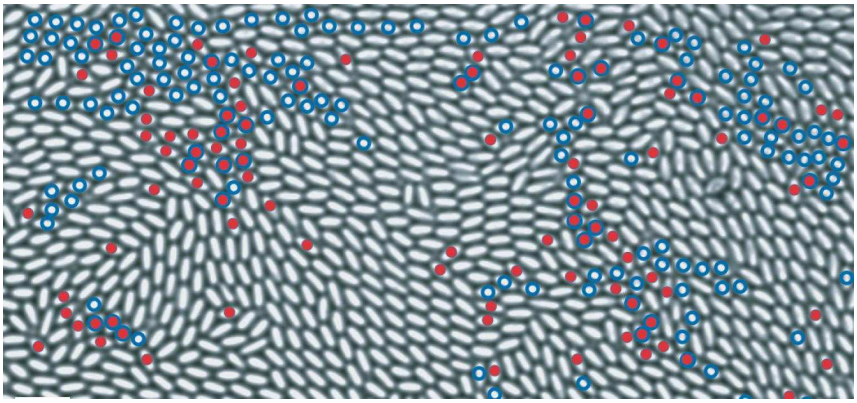

Figure 3.25: Top 10 % orientationally (solid) and translationally (hollow) most-mobile particles at $\Delta u = 1.16$ and $\phi = 0.81$.

laws can be readily extended to systems with short-range attraction as well. Interestingly, quasi-long ranged ordering is promoted at intermediate Δu's and results in a two-step glass transition with an intervening orientational glass regime. Although our experiments showed clear reentrant behaviour only in the translational DoF, it would be worthwhile to investigate the role of α on reentrant glass dynamics. Further, it would be of immense interest to quantify dynamics in the vicinity of the A_3 singularity[8–10] in glasses of colloidal ellipsoids.

Bibliography

[1] Z. Zheng, F. Wang, and Y. Han, Phys. Rev. Lett. **107**, 065702 (2011).

[2] M. Letz, R. Schilling, and A. Latz, Phys. Rev. E **62**, 5173 (2000).

[3] K.N. Pham, A.M. Puertas, J. Bergenholtz, S.U. Egelhaaf, A. Moussaid, P.N. Pusey, A.B. Schofield, M.E. Cates, M. Fuchs, and W.C.K. Poon, Science **296**, 104 (2002).

[4] T. Eckert and E. Bartsch, Phys. Rev. Lett. **89**, 125701 (2002).

[5] A. Latka, Y. Han, A.M. Alsayed, A.B. Schofield, A.G. Yodh, and P. Habdas, Europhys. Lett. **86**, 58001 (2009).

[6] L.J. Kaufman and D.A. Weitz, J. Chem. Phys. **125**, 074716 (2006).

[7] N.B. Simeonova, R.P.A. Dullens, D.G.A.L. Aarts, V.W.A. de Villeneuve, H.N.W. Lekkerkerker, and W.K. Kegel, Phys. Rev. E **73**, 041401 (2006).

[8] K.A. Dawson, G. Foffi, F. Sciortino, P. Tartaglia, and E. Zaccarelli, J. Phys.: Condens. Matter **13**, 9113 (2001).

[9] A.M. Puertas, M. Fuchs, and M.E. Cates, Phys. Rev. Lett. **88**, 098301 (2002).

[10] K. Dawson, G. Foffi, M. Fuchs, W. Gotze, F. Sciortino, M. Sperl, P. Tartaglia, Th. Voigtmann, and E. Zaccarelli, Phys. Rev. E **63**, 011401 (2000).

[11] E. Zaccarelli and W.C.K. Poon, Proc. Nat. Acad. Sci. **106**, 15203 (2009).

[12] W. Gotze and L. Sjogren, Rep. Prog. Phys. **55**, 241 (1992).

[13] W. Gotze, J. Phys.: Condens. Matter **2**, 8485 (1990).

[14] W. Kob and H. C. Andersen, Phys. Rev. Lett. **73**, 1376 (1994).

[15] P. Pfeiderer, K. Milinkovic, and T. schilling, Europhys. Lett. **84**, 16003 (2008).

[16] G. Adam and J.H. Gibbs, J. Chem. Phys. **43**, 139 (1965).

[17] E.R. Weeks, J.C. Crocker, A.C. Levitt, A. Schofield, and D.A. Weitz, Science **287**, 627 (2000).

[18] T. Narumi, S.V. Franklin, K.W. Desmond, M. Tokuyama, and E.R. Weeks, Soft Matter **7**, 1472 (2011).

[19] Y. Han, A.M. Alsayed, J. Zhang, T.C. Lubensky, and A.G. Yodh, Science **314**, 626 (2006).

[20] S.C. Glotzer, J. Non-Cryst. Solids **274**, 342 (2000).

[21] C. Donati, S.C. Glotzer, P.H. Poole, W. Kob, and S.J. Plimpton, Phys. Rev. E **60**, 3107 (1999).

[22] A.S. Keys, A.R. Abate, S.C. Glotzer, and D.J. Durian, Nature Phys. **3**, 260 (2007).

[23] G. Brambilla, D. El Masri, M. Pierno, L. berthier, L. Cipelletti, G. Petekidis, and A.B. Schofield, Phys. Rev. Lett. **102**, 085703 (2009).

[24] T. Shen, C. Schreck, B. Chakraborty, D.E. Freed, and C.S. O'Hern, Phys. Rev. E **86**, 041303 (2012).

[25] S. Asakura and F. Oosawa, J. Chem. Phys. **22**, 1255 (1954).

[26] S. Kruger, H.J. Mogel, M. Wahab, and P. Schiller, Langmuir **27(2)**, 646 (2011).

[27] A. Sheu and S.A. Rice, Phys. Rev. E **72**, 011407 (2005).

[28] J.R. Savage, D.W. Blair, A.J. Levine, R.A. Guyer, and A.D. Dinsmore, Science **314**, 795 (2006).

[29] J.A. Cuesta and D. Frenkel, Phys. Rev. A **42**, 2126 (1990).

List of Publications

"Depletion Attraction Induced Two-Step Glass Transition in Short Colloidal Ellipsoids", Chandan K. Mishra, Amritha Rangrajan, Rajesh Ganapathy, Accepted **Phys. Rev. Lett.**, March 2013.